https://ntrs.nasa.gov/search.jsp?R=19720018366 2020-03-23T12:18:32+00:00Z

NASA TECHNICAL MEMORANDUM

NASA TM X-62,157

NASA TM X-62,157

N

(NASA-TM-X-62157) TRANSONIC TRANSPORT STUDY: STRUCTURES AND AERODYNAMICS M.D. Ardema, et al (NASA) Jun. 1972 84 p CSCL 01B

N72-26016

Unclas
G3/02 32610

TRANSONIC TRANSPORT STUDY – STRUCTURES AND AERODYNAMICS

Mark D. Ardema and Louis J. Williams

Office of Aeronautics & Space Technology
Advanced Concepts & Missions Division
Moffett Field, Ca. 94035

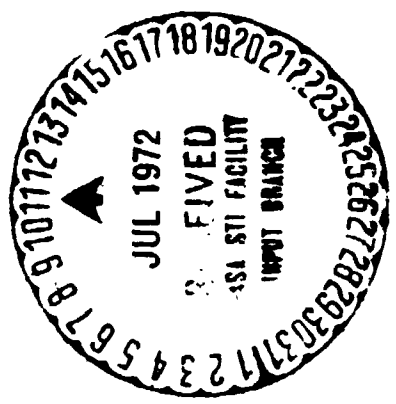

NATIONAL AERONAUTICS AND SPACE ADMINISTRATION

WASHINGTON, D. C. JUNE 1972

TABLE OF CONTENTS

SUMMARY

This paper presents the structural and aerodynamic aspects of a general study of advanced transonic transports. In this study, aircraft designed to cruise at Mach numbers of 0.90, 0.98, and 1.15 were comparatively analyzed. The wings of all three aircraft employ supercritical sections, and the two aircraft with the highest cruise Mach numbers also employ fuselage area ruling.

Structural/aerodynamic characteristics and interactions are investigated both parametrically and with the aid of an automated configuration optimization program. The effects of replacing conventional aluminum airframe structure by advanced filamentary composite (carbon/epoxy) structure receive particular attention. The methods employed in the structural/aerodynamic analysis are presented in the appendices.

INTRODUCTION

It is well known that the commercial transport aircraft industry is a vital part of the nation's economy. In order to maintain the present U. S. dominance in this field in the face of rising foreign competition, the next generation of transport designs must incorporate the latest and best of advanced technology. For this reason, a study was initiated to examine commercial transport aircraft, designed for introduction in approximately 1980, for the primary purpose of determining the advanced technology areas that give the largest improvements in performance and economics over current aircraft. The results of this study are reported in a summary paper (ref. 1) and papers in the specialty areas of aerodynamics and structures, propulsion (ref. 2), and economics (ref. 3). This paper reports the methods used and the results obtained in the areas of aerodynamics and structures.

The study is limited to transcontinental aircraft which would not produce a sonic boom on the ground. The aircraft studied are conventional swept wing/fuselage configurations designed for a range of 2700 n. mi. with a payload of 200 passengers and no cargo.

One effect investigated was that of increasing cruise speed. Increased cruise speed is valuable, not only because of a possible competitive market advantage, but also because of the resulting increased aircraft productivity. Aircraft were studied that are designed to cruise at Mach numbers of 0.90, 0.98, and 1.15. For the purposes of this study the aircraft are denoted respectively as CVT (conventional transport), ATT (advanced technology transport), and TST (transonic transport). Cruise at Mach number 0.90 represents approximately the highest cruise speed achievable without significant wave drag for an aircraft using the supercritical wing and no fuselage area ruling. Cruise at Mach number 0.98 represents approximately the highest cruise speed achievable without wave drag by using the supercritical wing and fuselage area ruling.

A cruise speed of Mach number 1.15 is of interest because it represents approximately an upper limit for cruise with no sonic boom reaching the ground. Because temperatures at cruise altitude are lower than those at sea level, the speed of sound is lower and as a result an aircraft flying at Mach 1.15 at 40,000 feet is actually flying at a velocity that corresponds to Mach 1 at sea level. Both theory and flight tests indicate that no boom is heard on the ground under these conditions. Recent results suggest that Mach 1.15 may be too high; Mach 1.08 may be more reasonable to allow for terrain and weather fluctuations encountered in flying across the country. A cruise Mach number of 1.08 at 40,000 feet would correspond to a sea level Mach number of 0.94. For the purposes of this study, it is felt that the results pertaining

to the aircraft designed to cruise at Mach 1.15 would be very close to those for an aircraft designed to cruise at Mach 1.08.

The aircraft of this study were analyzed with the aid of TRANSYN-TST, an aircraft synthesis program developed by ACMD personnel. The TRANSYN-TST computer program consists of a control program and a number of subroutines to do the varicus specialty tasks required to synthesize an aircraft design. Comparisons were facilitated by using the same computing methods and ground rules (range and payload requirements) for all aircraft. The methods used in the aerodynamic and structures subroutines of TRANSYN-TST are described in detail in the appendices.

The studies of advanced aerodynamics technology involved application of the supercritical wing, which was developed by Dr. R. Whitcomb at Langley Research Center. With this wing it is possible to delay the onset of wave drag and/or to use thicker wing sections with lower wing sweep. Proper fuselage area ruling was used to minimize the wave drag for the aircraft designed to cruise at Mach 1.15 and to eliminate it for the aircraft designed to cruise at Mach 0.98. In the structures/materials area, the effect of advanced composite materials on aircraft structural weight and performance was investigated. In particular, the effect on gross takeoff weight of using carbon/epoxy composite material in the primary load carrying structure was analyzed. Combining advanced structures technology with advanced aerodynamics leads to interesting tradeoffs in aircraft design. For example, more efficient structures allow the aircraft to be designed to achieve higher aerodynamic efficiency. These structures and aerodynamic interactions are described in this report.

METHODS OF ANALYSIS

Structures

Traditionally, preliminary weight estimates of aircraft are made using empirical methods based on the weights of existing aircraft. These methods, however, are undesirable for studies of the type reported here for two reasons. First, since the weight estimating formulas are based on existing conventional aircraft, their application to unconventional configurations (e.g., those with area ruled bodies) is suspect. Secondly, they provide no straightforward manner for assessing the impact of advanced technology structures and materials (e.g., filamentary composite materials). For the present study the weights of the load carrying wing and fuselage structures were determined by analytically based methods. Since it was necessary to be able to rapidly evaluate a large number of specific designs, the methods employed were based on idealized vehicle models and simplified structural analysis.

The configurations considered in this study are of the conventional wing-body type. As shown schematically in figure 1, the fuselage structure is an integrally stiffened shell stabilized by frames and the structure is sized by longitudinal bending. The wing is a multi-web box beam designed by span-wise bending and shear. The lower portion of the wing-fuselage carry-through structure carries the span-wise bending, shear, and torsion loads introduced by the outboard portion of the wing; the entire carry-through structure carries longitudinal bending loads.

The method of determining the fuselage structural weight is based on simple beam theory and is described in Appendix A. The bending moment

distribution resulting from a 2.5 g maneuver is computed first. The analysis then proceeds on a station-wise basis, calculating the minimum amount of material at each longitudinal station to satisfy static strength and stability requirements. The fuselage shell is sized by buckling with a compression strength cut-off. In addition, the shell is checked for minimum gage and tensile strength requirements and resized if necessary. For the buckling analysis, the integrally stiffened shell is analyzed as a wide column and the frames are sized by the Shanley criterion.

The wing weight analysis is described in Appendix B. The weight of the structural wing box is determined by calculating the minimum amount of material required to satisfy static buckling requirements at a series of span-wise stations. The covers of the multi-web box are sized by buckling due to local instability and the webs by flexure-induced crushing. Required shear material is computed independently of buckling material. Aeroelastic effects are not accounted for directly. For the carry-through structure, buckling, shear, and torsion material are computed independently and summed.

The weight analyses of the fuselage and wing described above do not completely account for the total weight of these structures. Specifically, weight penalties due to fasteners, cutouts, surface attachments, uniform gage requirements, manufacturing constraints, aeroelastic effects, etc., have not been directly determined. These weight items, commonly aggregated in a term called "non-optimum" weight, are determined by an empirical method based on existing aircraft, as described in Appendix A. The resulting "non-optimum factors," are 2.9 for the fuselage and 2.6 for the wing.

The weights of all the other items making up the dry weight of the study aircraft are estimated by empirical formulas derived from

regression analysis of existing aircraft. Such formulas predict the weight of these items satisfactorally for comparative studies.

The structural and weight analysis methods were used to estimate the weights of two existing aircraft, the 707-120B and the 747B, and the results are compared with the actual weights in figure 2. These aircraft were not used in the regression analyses to determine the non-optimum factors and therefore the comparison provides a good check on the methods. The agreement is considered excellent for the 707-120B and good for the 747B. The descrepancy in the case of the 747B is primarily in the fuselage weight, and may be because the 747B airframe is a more recent design than the airframes of the 707-120B and the aircraft used in the regression analyses.

Aerodynamics

The methods used to estimate the lift and drag characteristics of the study aircraft are described in detail in Appendix D and summarized in figure 3. The major differences between the study aircraft configurations are shown in figure 4. These factors determined the aerodynamic methods which were applied. The wing sweep angles chosen for each configuration resulted from constraining the Mach number perpendicular to the wing quarter chord line to 0.74. This constraint and a constraint of 10% on the wing thickness ratio normal to the wing quarter chord were applied to insure good wing section performance. These aerodynamic constraints are shown as a function of cruise Mach number in figure 5.

In order to compare the relative landing qualities of the study aircraft, the performance of each aircraft with high-lift devices was estimated. A computer program based on the relationships described in reference 4 was used to calculate the effectiveness of high-lift devices on various wings

with different wing sweep, aspect ratio, taper ratio, and thickness ratio. All configurations were analyzed with the same type of high-lift devices, double slotted trailing edge Fowler flaps and leading edge slats. The aircraft approach speed was computed at 1.3 times the aircraft stall speed, based on the estimated maximum lift coefficient ($C_{L_{MAX}}$) and an aircraft maximum landing weight with 0.7 of the mission fuel consumed.

CHARACTERISTICS OF NOMINAL VEHICLES

The nominal aircraft configurations are shown in figure 6. All the aircraft were designed for a range of 2700 nautical miles with a payload of 200 passengers and no cargo. The nominal values of aspect ratio, wing loading, and engine bypass ratio are 7,120 lbs/ft^2, and 2, respectively. The aircraft are drawn to scale to show the relative sizes and the effect of fuselage area ruling. The gross takeoff and operating empty weights are 235,000 lbs and 130,000 lbs for the CVT, 250,000 lbs and 140,000 lbs for the ATT, and 600,000 lbs and 235,000 lbs for the TST. Thus, due primarily to wave drag, the TST is significantly heavier than the other two configurations.

The principal difference in the fuselage structure of the configurations considered here and those of current subsonic jet transports is the presence of fuselage area ruling. As mentioned earlier, the M 1.15 vehicle (TST) and the M 0.98 vehicle (ATT) are area ruled, whereas the M 0.90 vehicle (CVT) is not. Since the TST is the most highly area ruled of the configurations, this configuration will be used to illustrate the effects of area ruling on body structural weight.

The wave drag encountered by the TST results in a large fuel requirement which leads to a high gross takeoff weight (nearly three times that of the

other study configurations). Aerodynamic support of this high weight requires a large wing. Thus the fuselage of this configuration is relatively highly loaded and severely area ruled when compared to the CVT and the ATT. Figure 7a shows the body contour; the area ruling is clearly seen. Figure 7b shows the distribution of longitudinal bending moment on the body. Note that this distribution has a sharp peak which occurs over the area ruled portion of the body. Since body shell weight per unit surface area, which is shown in figure 7c, increases with increasing bending moment and decreases with increasing radius, this weight is large in the area ruled portion of the body, especially aft of the wing carry-through structure. (Recall that this structure helps to carry the longitudinal bending loads.) The bump in the unit weight at the aft end of the body is due to introduction of the tail load. However, the effect of the increase in unit weight at this body station on the overall fuselage structure weight is small because of the relatively small fuselage diameters in this region. The shell is sized by the minimum gage constraint at the front of the fuselage and by buckling elsewhere, except in the region of the peak bending moments where the compression strength cutoff is active.

The principal differences in the wing structure of the configurations considered here and those of current subsonic transports are higher sweep, higher aspect ratio, and thicker supercritical wing airfoil sections. The higher sweep and aspect ratio result in relatively higher wing weights for the study configurations in spite of the greater wing thickness. The "optimized" configurations employing advanced composite materials have particularly high aspect ratios, significantly higher than existing transport aircraft. Since aeroelastic effects have not been accounted for directly (they have been accounted for indirectly for moderate aspect

ratios through the "non-optimum" factor), the wing weight estimates for these configurations must be regarded as possibly optimistic.

SENSITIVITIES OF NOMINAL VEHICLES TO CONFIGURATION PARAMETERS

The sensitivities of the previously discussed nominal configurations will be presented in the form of variations in airframe weights, $(L/D)_{MAX}$, and gross takeoff weight (W_{GTO}) with changes in the configuration parameters aspect ratio (AR), wing loading (W/S), thickness ratio (t/c), and sweep (Λ). In each variation, the parameters not being changed are held constant at their nominal values. The payload-range characteristics of the vehicles are also held constant at their nominal values (200 passengers, 2700 n. mi.). Operating weight empty fraction (OWE/W_{GTO}) and $(L/D)_{MAX}$ are used as measures of aircraft structural efficiency and aerodynamic efficiency, respectively. It should be noted, however, that because of the resizing process a large change in OWE will result in only a small change in OWE/W_{GTO}. Configuration gross weight, which is closely related to direct operating cost, is used to indicate overall aircraft efficiency.

The sensitivities of the wing, fuselage, and OWE weight fractions to AR are shown in figure 8a. The wing weight fraction increases with increasing AR due to increasing span; the fuselage weight fraction increases due to decreasing root chord and also, for the ATT and TST, due to increasingly severe fuselage area ruling. The sharp uptrend for the TST above AR = 7 is a size effect in which attempts to accomplish the mission by increasing the aircraft gross weight are overbalanced by increasing structural weight. Above AR = 8, the TST cannot carry 200 passengers 2700 n. mi. at any gross weight. The effect for all configurations is increased OWE

fraction with increasing AR. However, AR also has a strong effect on $(L/D)_{MAX}$ as shown in figure 8b, and the increasing aerodynamic efficiency with increasing AR (due to reduced induced drag) tends to balance the decreasing structural efficiency, with the result that W_{GTO} is relatively insensitive to AR for the CVT and the ATT. The TST, being marginally able to perform the mission, is sensitive to almost any parameter, and the TST gross weight exhibits a sharp minimum at about the nominal value.

The wing weight fraction, figure 9a, decreases with increasing W/S due to decreasing wing area. The fuselage weight fraction varies only slightly due to changing root chord length and fuselage area ruling, except for the TST. The net effect is increasing structural efficiency (decreasing OWE weight fraction) with increasing W/S. However, since $(L/D)_{MAX}$ decreases with increasing W/S, the situation is the same as for AR; the structural and aerodynamic effects tend to neutralize each other and W_{GTO} is relatively insensitive to W/S (figure 9b). The exception is the TST which improves with higher W/S. This trend, however, is constrained by landing speed limitations; the effect on landing quality is considered later in this paper when "optimized" configurations are discussed.

Figure 10a shows that wing weight fraction increases slightly with decreased t/c. The fuselage weight fraction decreases slightly for the area ruled ATT and TST configurations because a thinner wing results in a less severely area-ruled body. The OWE fraction is relatively insensitive to t/c. Since $(L/D)_{MAX}$ is also very insensitive to t/c within reasonable limits, as shown in figure 10b, this parameter is relatively unimportant for configuration optimization, and t/c was held at the aerodynamically constrained upper limit for each configuration throughout the study.

Figure 11a shows that wing weight fraction increases with increasing Λ while fuselage weight fraction remains fairly constant. The TST again

is much more sensitive than the other configurations. Since the lowest W_{GTO} occurred at the aerodynamically constrained minimum sweep value, as shown in figure 11b, the sweep was held at this minimum value for each configuration throughout the study.

ADVANCED COMPOSITE MATERIALS

Because the best prospect for substantially improving the performance of aircraft appears to be the use of advanced composite materials, the potential impact on transport aircraft performance of these materials was investigated in this study. Two advanced composites materials were considered: boron filaments in an epoxy matrix (B/E) and carbon filaments in an epoxy matrix (C/E). For the purposes of this study, it was assumed that these materials are layed up in isotropic laminates consisting of orthotropic lamina, each lamina being composed of unidirectional filaments in a homogeneous matrix. The manner in which the material properties of the composites were characterized is derived and discussed in Appendix C. Only complete substitution of composite materials in both the wing and fuselage load carrying structures was considered in the present study. It should be noted that selective substitution may be more cost effective than total substitution and that composite materials may also be attractive for use in other structures such as tails and landing gear.

Before investigating the effect of composite materials on the study configurations, it is instructive to consider the material properties as given in Table C1 of Appendix C. In the last column, $\rho/\sqrt{E}$ is tabulated with respect to aluminum alloy; this quantity is a good indicator of the

weight of buckling critical structures. The table indicates that a composite, buckling critical structure will be about 60% of the weight of an equivalent aluminum alloy structure. Since the weight of strength critical structure is proportional to ρ/F, the table indicates that strength critical structure will show an even greater weight reduction with the use of advanced composites than will buckling critical structure.

The weights which result when the wing and fuselage structures are made entirely of C/E are shown in Table 1 and compared with the weights of the same size aluminum airframes. Since these configurations were analyzed at the same gross takeoff weight, the aircraft which results in lower operating weight empty (OWE) will be able to carry more fuel and thus have longer range with the same payload. The net reductions in wing and fuselage weights for the three configurations range from 33% to 43%. This translates into reductions of from 15-1/2% to 19-1/2% in the OWE. The reduction is largest for the TST because this vehicle is heavier and more highly loaded than the other two vehicles and thus is more strength critical.

Rather than hold gross takeoff weight constant during the material substitution, it is more interesting to see the effect of the substitution when holding the payload and range fixed. In this substitution, the magnification effect (lower structural weight means lower fuel weight means lower structural weight, etc.) is accounted for. Figure 12 shows that composites reduce the gross weight of the nominal CVT slightly (15%), the nominal ATT slightly more (19%) and the nominal TST substantially (48%). In every case, the C/E composite is better (lighter weight) than the B/E, as is also obvious from Table C1. Therefore, further analysis of C/E was emphasized in the present study. The gross takeoff weights of the CVT

and ATT are signficantly less than that of the TST, even when the latter is made of composite material. Since the airframe cost of an aircraft made from advanced composite materials will be different than the cost of a conventional aluminum alloy aircraft, material selection must be based on overall cost effectiveness, and not solely on the basis of least weight. It is clear, however, that the TST is a much more attractive vehicle when made of C/E than when made of aluminum.

The sensitivities of the gross takeoff weights (for the specified mission of 2700 n. mi. with 200 passengers) of the C/E configurations to the configuration parameters $\mathcal{R}$, W/S, t/c, Λ are shown on figures 13-16. Also shown for reference are the sensitivities of the aluminum configurations discussed earlier. Sensitivity of gross takeoff weight to $\mathcal{R}$, figure 13, shows the same affect for C/E as for aluminum in the case of the CVT and ATT. For the TST, the C/E configuration is much less sensitive to $\mathcal{R}$. The $(L/D)_{MAX}$ is less for the lighter C/E configurations than for the corresponding aluminum configurations due to the smaller relative wing area and fixed fuselage size (wing loading is held constant). Substitution of C/E for aluminum results in little change in sensitivity to W/S, figure 14. The C/E TST, however, is much less sensitive to W/S than is the aluminum TST, but least weight still results at higher W/S than nominal. The material substitution has the same affect on the sensitivities to t/c, figure 15, and to Λ, figure 16, as it had on the sensitivities to $\mathcal{R}$ and W/S; the CVT and ATT remain relatively insensitive while the C/E TST becomes much more insensitive than the aluminum TST.

OPTIMIZED CONFIGURATIONS

As has been shown, the vehicles of this study have strong structural/aerodynamic interactions and in many cases structural efficiency may be traded for aerodynamic efficiency. To investigate these interactions, the synthesis program was coupled with a parameter optimization program called AESOP (refs. 5 and 6). AESOP adjusted the values of AR, W/S, and engine bypass-ratio to obtain minimum W_{GTO}. The parametric results presented earlier show that t/c and Λ are best at their constrained values and therefore these parameters were not allowed to vary in the optimization. Gross takeoff weight was chosen as the quantity to be minimized since it also closely reflects the direct operating cost (unless materials are changed). Since some unconstrained configurations optimized at high W/S and low AR which gave high landing speeds, the affect of a performance penalty for landing speed was also investigated. Consideration of optimized configurations is particularly important when evaluating aircraft made of composite structure because the optimum configurations of these aircraft may be considerably different than for aircraft made of aluminum. Thus, the resultant weight advantage of composite materials might be considerably greater than that predicted by substitution without configuration reoptimization.

Six configurations were optimized in the manner just described. These configurations utilized the two materials aluminum (Al) and C/E for the three study vehicles CVT, ATT, and TST. The weight breakdowns of the configurations are shown on figure 17; also shown for comparison are the weights of the nominal configurations. The gross takeoff weights of the CVT and ATT, Al and C/E configurations have been reduced by about 5% relative to the nominal configurations. The weight of the Al TST has

been reduced by about 15%. However, the weight of the C/E TST has not been reduced relative to the nominal due to the fact that the wing size of this configuration is limited by a minimum fuel volume constraint. It is significant that the relative ranking in terms of gross weight of the configurations is the same for the optimized configurations as for the nominals. As was expected, gross weight is insensitive to the configuration parameters in the vicinity of the optimums.

Drawings and some of the important parameters of the three optimized Al and C/E aircraft are shown in figures 18 and 19, respectively. In redesigning the aircraft with C/E material, the increased structural efficiency allowed increased aerodynamic efficiency. Optimization of the aircraft configuration for each case insured that the best balance between weight and aerodynamics was obtained. The largest reduction in aircraft gross takeoff weight due to the use of C/E material was for the TST configuration. As mentioned previously, this is partly because the Al TST is operating close to its ultimate mission capability.

For all configurations the use of C/E results in an increase in the optimum wing aspect ratio. The aspect ratio of the CVT increased from 6.8 to 9.1 with C/E, that of the ATT increased from 8.1 to 12.4, and that of the TST went from 6.4 to an aspect ratio of 9.8. At the same time, the optimum W/S decreased in all cases: from 123 to 113 psf for the CVT, 123 to 106 psf for the ATT, and 127 to 100 psf for the C/E TST compared with the Al TST. Since the increased structural efficiency results in large AR for the C/E configurations, questions as to possible flutter problems arise. As stated previously, the present TRANSYN-TST synthesis program does not contain any flutter calculation, and no additional structural weight is added to increase the wing stiffness to avoid flutter.

Because of the lower wing loadings and higher aspect ratios of the optimized C/E configurations, their approach speeds are lower than for the optimized Al configurations. The effect is strongest in the case of the TST, where the approach speed has decreased from 190 knots for the Al TST to 168 knots for the C/E TST. The effects of W/S, $\mathcal{A}$R, and Λ on the $C_{L_{MAX}}$ and the resultant effect on approach speed for the three nominal aluminum configurations are shown in figures 20, 21 and 22. As mentioned previously, the approach speeds of all configurations were estimated for double slotted flaps and leading edge slats.

Using the parameter optimizer AESOP and including a performance penalty for high approach speed results in a change in the optimized Al ATT as shown in figure 23. On the left of the figure is the ATT configuration optimized without a penalty for high landing speed and on the right is the ATT configuration optimized with the landing speed penalty. The result of including this penalty is to increase the $\mathcal{A}$R and decrease the W/S. These design changes result in a slightly higher W_{GTO} because of the higher operating weight empty due to the increased wing and fuselage structural weight. The decrease in approach speed is substantial, from 170 knots for the unconstrained Al ATT to 151 knots for the constrained Al ATT. Figure 24 shows the affect of an approach speed constraint on the optimized C/E TST configuration. As with the ATT, the inclusion of this penalty for high landing speed results in higher $\mathcal{A}$R and lower W/S and leads to higher operating weight empty and higher W_{GTO}. The decrease in approach speed is less for the TST than the ATT, having dropped from 168 knots to 158 knots. Because of the large penalty in overall performance of this small landing speed reduction, possible consideration should be given to other means of obtaining high-lift at takeoff and landing, such as variable geometry.

CONCLUDING REMARKS

The structural/aerodynamic characteristics of advanced transonic transports have been investigated. Specifically, aircraft designed to cruise at Mach numbers of 0.90 (CVT), 0.98 (ATT), and 1.15 (TSS) were studied. It was found that the CVT and ATT designs had similar characteristics and performance (as measured by gross takeoff weight) for the same payload/range requirements (200 passengers, 2700 n. mi.). The principal difference between the CVT and the ATT is the use of area ruling in the latter, resulting in a slight increase in fuselage structural weight. The gross takeoff weight of the TST, however, was found to be more than twice that of the other two designs for the same mission if all designs employ conventional aluminum airframes. The reason for the poor performance of the TST is the large wave drag of this configuration.

Parametric analyses were made for the three designs. These analyses show that both aspect ratio and wing loading had strong effects on aerodynamic efficiency as measured by $(L/D)_{MAX}$ and structural efficiency as measured by operating weight empty. However, these effects tended to cancel each other and the net effect of changes in either parameter on the gross takeoff weight was small. The parametric results also showed that the values of wing sweep and thickness-to-chord ratio should be held at their aerodynamically constrained values.

Most important of the advanced technologies investigated was that of advanced composite materials. Substitution of carbon/epoxy material for aluminum in both the wing and fuselage primary structure (without resizing

the configurations) resulted in 35-40% reductions in the weights of these structures. This translated into 15-20% reductions in operating weight empty. If the composite designs are resized to the same payload/range criteria as the aluminum ones, the change to composite material results in decreases in gross takeoff weight of 15% for the CVT, 19% for the ATT, and 48% for the TST.

Six configurations (consisting of the three designs CVT, ATT, and TST made of the two materials aluminum and carbon/epoxy) were "optimized" with the aid of a parameter optimization program. In this optimization, the values of aspect ratio, wing loading, and engine bypass-ratio were altered to obtain minimum gross takeoff weight, both with and without an approach speed constraint. As expected, the gross takeoff weight is insensitive to variations in the configuration parameters in the vicinity of the optimums. For all three vehicle designs the use of carbon/epoxy as opposed to aluminum results in a higher value of the optimum wing aspect ratio due to increased structural efficiency being traded for increased aerodynamic efficiency. Introduction of an approach speed constraint results in modest performance penalties for the ATT configurations but, due to high wing sweep, severe penalties for the TST configurations.

REFERENCES

1. Williams, Louis J.: "Transonic Transport Study - Summary," NASA TM X-62,156, May 1972.

2. Waters, Mark H.: "Transonic Transport Study - Propulsion Systems," NASA TM X-62,158, May 1972.

3. Smith, Cynthia L., and Wilcox, Darrell E.: "Transonic Transport Study - Economics," NASA TM X-62,159, May 1972.

4. Sanders, Karl L.: "High-Lift Devices, A Weight and Performance Trade-Off Methodology," Tech. Paper No. 761, The Society of Aeronautical Weight Engineers, Inc., May 1969.

5. Hague, D. S., and Glatt, C. R.: "An Introduction to Multivariable Search Techniques for Parameter Optimization (and Program AESOP)," NASA CR-73200, April 1968.

6. Hague, D. S., and Glatt, C. R.: "A Guide to the Automated Engineering and Scientific Optimization Program - AESOP," NASA CR-73201, June 1968.

7. Ardema, Mark D.: "Structural Weight Analysis of Hypersonic Aircraft," NASA TN D-6692, March 1972.

8. Ardema, Mark D.: "Analysis of Bending Loads of Hypersonic Aircraft," NASA TM X-2092, October 1970.

9. Shanley, F. R.: "Weight-Strength Analysis of Aircraft Structures," Dover, 1960.

10. Crawford, R. F., and Burns, A. B.: "Strength, Efficiency, and Design Data for Beryllium Structures," ASD Technical Report 61-692.

11. Dow, N. F., and Rosen, B. W.: "Structural Efficiency of Orthotropic Cylindrical Shells Subjected to Axial Compression," AIAA Journal, March 1966.

12. Ashton, J. E.; Halpin, J. C.; and Petit, P. H.: "Primer on Composite Materials Analysis," Technomic, 1969.

13. Whitney, J. M., and Riley, M. B.: "Elastic Properties of Fiber Reinforced Composite Materials," AIAA Journal, Vol. 4, No. 9, September 1966.

14. Crawford, R. F.: "Efficiency of Boron- and Carbon-Polymer Laminated Film Composites for Stability-Design Structures," AIAA Paper No. 71-353; presented at 12th AIAA/ASME Structures, Structural Dynamics, and Materials Conference.

15. Tsai, S. W., and Pagano, N. J.: "Invariant Properties of Composite Materials," Composite Materials Workshop, edited by Tsai, S. W.; Halpin, J. C.; Pagano, N. J.; Technomic, 1968.

16. Adams, O. F., and Doner, D. R.: "Transverse Normal Loading of a Unidirectional Composite," J. Composite Materials, Vol. 1, 1967.

17. Woodward, F. A.: "Analysis and Design of Wing-Body Combinations at Subsonic and Supersonic Speeds," J. of Aircraft, Vol. 5, Nov.-Dec. 1968.

18. Koelle, Heinz Hermann: "Handbook of Astronautical Engineering," McGraw-Hill Book Company, Inc., 1961.

19. Miele, A.: "Theory of Optimum Aerodynamic Shapes," Academic, 1965.

20. Williams, L. J.: "Estimated Aerodynamics of All-Body Hypersonic Aircraft Configurations," NASA TM X-2091, March 1971.

21. Jones, R. T.: "The Minimum Drag of Thin Wings in Frictionless Flow," Journal of Aero. Sci., Feb. 1951, pp. 75-81.

22. Kuchemann, D.: "Aircraft Shapes and Their Aerodynamics for Flight at Supersonic Speeds," Proceedings of the Second International Congress for the Aero. Sci., Advances in the Aero. Sci., Vol. 3, pp. 221-249, A Pergamon Press Book, The Macmillan Co., N. Y., 1962.

23. Lock, R. C.: The Aerodynamic Design of Swept Winged Aircraft at Transonic and Supersonic Speeds," J. Royal Aero. Sco., June 1963, pp. 325-336.

APPENDIX A - BODY WEIGHT ANALYSIS

In this appendix, the methods used to estimate the body weights of the study configurations are presented. These methods are the same as those presented in reference 7, and will only be given briefly here. Only configurations with circular cross-sections are considered.

The first step in determining body weight is computation of the longitudinal bending moment distribution. To this end the longitudinal weight and lift distributions and vehicle center of gravity are computed using the body profile, R(X), determined as described in Appendix E, and the wing (see Appendix B), tail, and propulsion system weights. The longitudinal bending moment distribution is then obtained by considering vehicle loading due to a static 2.5g pull up maneuver (factor of safety of 1.5). See reference 8.

The bending moment M is used to compute at each longitudinal body station, x, the axial stress resultants at the point of maximum stress due to bending. These are, using the flexure formula for beams,*

$$N_x^- = \frac{MR}{I'_y} + N_x^a$$

$$N_x^+ = \frac{MR}{I'_y} + \frac{R\,P_g}{2} - N_x^a$$

for compression and for tension, respectively, where I'_y is the moment of inertia of the body shell divided by the thickness and N_x^a is the force per inch due to axial acceleration. Note that pressure loads are not used to relieve compressive stresses. The value of gage pressure, P_g = 8.77 psi, was held throughout the study. The stress resultant in the

*symbols are the same as in reference 7

circumferential direction is

$$N_y = R\, P_g\, K_p$$

where K_p accounts for the fact that not all of the shell material is available for resisting hoop stress. It is assumed that the shell material is uniformly distributed around the circumference.

The equivalent isotropic thicknesses of the shell are given by

$$\bar{t}_{S_C} = \frac{\bar{N}_x}{F_{CY}}$$

$$\bar{t}_{S_T} = \frac{1}{F_{TU}} \text{ MAX } (N_x^+, N_y)$$

$$\bar{t}_{S_G} = K_{g_w}\, t_{mg}$$

for designs limited by compression, tension, and minimum gage respectively where F_{CY} is the compressive strength and F_{TU} is the tensil strength. The material is assumed to have elasto-plastic behavior. A fourth thickness which must be considered is that for buckling critical structures, $\bar{t}_{S_B}$; expressions for this quantity will now be derived.

The nominal vehicles of this study have integrally stiffened shells stabilized by ring frames. In the buckling analysis of these structures, the shell is analyzed as a wide column and the frames are sized by the Shanley criteria (ref. 9). The buckling equation for wide columns (ref. 10) gives $\bar{t}_{S_B}$ as

$$\bar{t}_{S_B} = \sqrt{\frac{\bar{N}_x\, d}{E\, \epsilon_W}}$$

where d is the frame spacing and E is the modulus of elasticity. Values of the shell efficiency ϵ_W are given in Table B1. The Shanley criterion is based on the premise that the frames act as elastic supports for the wide column; this criterion gives the smeared equivalent isotropic thickness of the frames as

$$\bar{t}_{F_B} = 2 R^2 \sqrt{\frac{\pi C_F N_x}{K_{F1} d^3 E}}$$

where C_F is Shanley's constant and K_{F1} is a frame geometry parameter. See reference 7 for a discussion of the applicability of this criterion and for a detailed derivation of the equations presented here. If the structure is buckling critical, the total thickness is

$$\bar{t} = \bar{t}_{S_B} = \bar{t}_{F_B}$$

Minimizing $\bar{t}$ with respect to d results in

$$\bar{t} = \frac{4}{27^{\frac{1}{4}}} \cdot \left(\frac{\pi C_F}{K_{F1} \epsilon_W^3}\right)^{\frac{1}{8}} \left(\frac{N_x}{E}\right)^{\frac{1}{2}} (2R^2)^{\frac{1}{4}}$$

$$\bar{t}_{S_B} = \frac{3}{4} \bar{t}$$

$$\bar{t}_{F_B} = \frac{1}{4} \bar{t}$$

$$d = \left(6 R^2 \sqrt{\frac{\pi C_F \epsilon_W}{K_{F_1}}}\right)^{\frac{1}{2}}$$

so that the shell is three times as heavy as the frames.

At each fuselage station x, the shell may be sized by compression, tension, minimum gage, or buckling and the frames are sized by general instability. For minimum weight, it is desired to find the least total

thickness $\bar{t} = \bar{t}_S = \bar{t}_F$ as a function of d which satisfies the four conditions resulting from the combinations of shell and frame criteria. Three of these conditions are monotonically decreasing with respect to d and the fourth, the buckling condition, has a minimum. The minimum $\bar{t}$ is obtained by a simple search procedure. The "ideal" or analytical weight of the body structure is then obtained by summation as

$$W_I = 2 \pi \rho \sum_{\substack{\text{body} \\ \text{length}}} \bar{t}_i \, R_i \, \Delta x_i$$

where quantities subscripted i depend on x.

The "non-optimum" body weight (due to fasteners, cutouts, surface attachments, uniform gage penalties, manufacturing constraints, aeroelastic effects, etc.) has yet to be determined. This weight is computed by an empirical method. The analysis described above was applied to five existing aircraft and the factor was determined which, when multiplied by the "ideal" weight, gave the best fit with the actual weights. This factor, called the "non-optimum" factor, was found to be 2.9; thus the non-optimum portion of the weight is nearly twice the analytically determined weight.

APPENDIX B - WING WEIGHT ANALYSIS

The lifting planforms of the configurations of the present study are tapered, swept wings with straight leading and trailing edges. The wing structure was assumed to be a rectangular multi-web box beam with the webs running in the direction of the structural span.

The first step in computing the wing weight is the determination of the geometry of the structural wing box. In terms of the input parameters W_{TO}, (W/S), AR , R_{TAP} and Λ_{LE}, the dependent parameters wing area, span, root chord, tip chord, and trailing edge wing sweep are computed from

$$S = \frac{W_{TO}}{(W/S)}$$

$$b = \sqrt{AR\ S}$$

$$C_R' = \frac{2\ S}{b\ (1+R_{TAP})}$$

$$C_T = R_{TAP}\ C_R'$$

$$\tan \Lambda_{TE} = \tan \Lambda_{LE} + \frac{2\ C_R'}{b}\ (R_{TAP} - 1)$$

(See figure B1). It is assumed that the forward 15% and the aft 15% of the streamwise chord are required for controls and high lift devices, leaving 70% for the structural box. The intersection of this box with the body contours determines the location of the rectangular carry-through structure.

The dimensions of the structural box and of the carrythrough structure are now determined. (See figure B2). The structural semi-span, b_s, is assumed to be at the quarter-chord line, whose sweep is

given by

$$\tan \Lambda_S = \frac{3}{4} \tan \Lambda_{LE} + \frac{1}{4} \tan \Lambda_{TE}$$

Thus,

$$b_s = \frac{b - W_C}{2 \cos \Lambda_S}$$

The streamwise chord at any point on the wing is given by

$$r(\zeta) = C_R' - \frac{\zeta}{b/2} (C_R' - C_T)$$

In particular, at the wing-body intersection,

$$C_R = C_R' - \frac{W_C}{b} (C_R' - C_T)$$

The structural root and tip chords are

$$C_{SR} = .7\, C_R$$

$$C_{ST} = .7\, C_T$$

respectively. In terms of y, the structural and total chords are given by

$$r_s(y) = C_{SR} - \frac{y}{b_s} (C_{SR} - C_{ST})$$

$$r(y) = C_R - \frac{y}{b_s} (C_R - C_T)$$

and the thickness of the wing at any spanwise station y is

$$t(y) = R_t\, r$$

It is assumed that the fuel is carried within the wing structure; the volume of this structure is found as follows:

$$V_W = 2\int_0^{b_s} r_s(y)\, t(y)\, dy = (C_R R_t)\, C_{SR}\, W_C$$

$$= 1.4\, R_t \int_0^{b_s} \left[C_R - \frac{y}{b_s} (C_R - C_T) \right]^2 dy + 0.7\, R_t C_R^2 W_C$$

$$V_W = 1.4\, R_t b_s \left[C_R^2 - C_R\,(C_R - C_T) + \frac{1}{3}\,(C_R - C_T)^2 \right] + 0.7\, R_t C_R^{\,2}\, W_C$$

This equation is based on flat upper and lower surfaces and neglects the volume of the structure.

The weight analysis proceeds in a station-wise manner along the y (structural semi-span) coordinate. At each station, the lift load, center of pressure, inertia load, center of gravity, shear force and bending moment are computed. For the inertial load, it is assumed that the fuel weight W_{FT} is distributed uniformly with respect to wing volume so that the inertial load at y is $\frac{W_{FT}}{V_W} V(y)$ where V(y) is the volume outboard of y; this volume has centroid C_g (y) with respect to station y. An estimate of the wing structural weight is included in W_{FT} for this calculation but the calculation is not redone when the actual structural weight has been computed. It is assumed that the lift load is distributed uniformly over the wing planform area so that the lift load at y is (W/S) A(y) where A(y) is the area outboard of y; the centroid of this area is denoted C_p (y).

The shear force is

$$F_S(y) = n\, K_S \left[(W/S)\, A - \frac{W_{FT}}{V_W} V - \sum_{i=1}^{n_e} h(y_i - y)\, W_{e_i} \right]$$

where n_e is the number of engines mounted on the semispan, W_{e_i} is the weight of the $i^{\underline{th}}$ engine, y_i is the location of the $i^{\underline{th}}$ engine, and

$$h(y_i-y) = \begin{cases} 1, & y_i > y \\ \\ 0, & y_i < y \end{cases}$$

The bending moment is

$$M(y) = n K_S \left[(W/S) A C_p - \frac{W_{FT}}{V_W} V C_g - \sum_{i=1}^{n_e} h(y_i-y) W_{e_i} (y_i-y)\right]$$

for a static pitch-plane maneuver of load factor n.

The dimensions and weight of the structural box can now be calculated. Reference 10 indicates that the critical instability mode for multiweb box beams is simultaneous buckling of the covers due to local instability and of the webs due to flexure induced crushing. This reference gives the solidity of least weight multiweb box beams as

$$\Sigma = \epsilon \left(\frac{M}{z_S t^2 E}\right)^e$$

where ϵ and e depend on the cover and web geometries (see Table B1). The solidity is defined as

$$\Sigma = \frac{W'_{BEND}(y)}{\rho z_S t}$$

where W'_{BEND} is the weight of bending material per unit span and ρ is the material density.

The weight of shear material is

$$W'_{SHEAR}(y) = \frac{\rho F_S}{\sigma_S}$$

The optimum web spacing (see figure B2) is computed from

$$d_W = t \left[\frac{(1-2e_C)}{(1-e_C)\sqrt{2\,\epsilon_W}} \left(\frac{M}{z_S t^2 E}\right)^{\frac{2e_C-3}{2e_C}} \epsilon_C^{\frac{3}{2e_C}}\right]^{\frac{2e_C}{4e_C-3}}$$

The equivalent isotropic thicknesses of the covers and webs are

$$\bar{t}_C = d_W \left(\frac{M}{\bar{z}_S t \; E \; \varepsilon_C d_W} \right)^{\frac{1}{e_C}}$$

$$\bar{t}_W = t \sqrt{\left(\frac{M}{\bar{z}_S t^2 \; E} \right)^{(2 - \frac{1}{e_C})} \left(\frac{\varepsilon_C d_W}{t} \right)^{\frac{1}{e_C}} \left(\frac{2}{\varepsilon_W} \right)}$$

respectively, and the gage thicknesses are

$$t_{g_C} = K_{g_C} \; \bar{t}_C$$

$$t_{g_W} = K_{g_W} \; \bar{t}_W$$

Values of ε, e, ε_C, e_C, ε_W, K_{g_C}, K_{g_W} are found in Table B1 for various structural concepts (ref. 10). If the wing structural semi-span is divided into N equal segments, the total "ideal" weight of the wing box structure is

$$W_{BOX} = \frac{2 \; b_s}{N} \sum_{i=1}^{N} \left(W'_{BEND_i} + W'_{SHEAR_i} \right)$$

The wing carrythrough structure consists of torsion material in addition to bending and shear material. The bending material is computed in the same manner as that of the box except that only the longitudinal component of bending moment contributes, i.e. (let $t_o = t\,(o)$ and $M_o = M\,(o)$),

$$\Sigma_C = \varepsilon \left(\frac{M_o \cos \Lambda_S}{t_o^2 \; C_{SR} \; E} \right)^e$$

The weight of the bending material is then

$$W_{BEND_C} = \rho \; \Sigma_C \; C_{SR} \; t_o \; W_C$$

The quantities d_W, $\bar{t}_W$ and $\bar{t}_C$ are computed in the same manner as for the box. The weight of the shear material is ($F_{S_o} = F_S$ (o))

$$W_{SHEAR_C} = \rho \frac{F_{S_o}}{\sigma_S} W_C$$

The torque on the carrythrough structure is

$$T = M_o \sin \Lambda_S$$

and the weight of the torsion material is then

$$W_{TORSION_C} = \frac{\rho T (t_o + C_{SR}) W_C}{t_o C_{SR} \sigma_S}$$

Finally, the "ideal" weight of the carrythrough structure is computed from

$$W_C = W_{BEND_C} + W_{SHEAR_C} + W_{TORSION_C}$$

As is the case with the fuselage structural weight, "non-optimum" weight must be added to the ideal weight to obtain the wing structural weight. This weight was estimated by applying the above analysis to five existing aircraft and determining the factor which, when multiplied by the ideal weight, gave the best fit with the actual weights. The resulting expression is

$$W_{WING} = 2.6 (W_{BOX} + W_C)$$

APPENDIX C - COMPOSITE MATERIAL CHARACTERIZATION

The composite materials considered in this paper consist of orthotropic lamina formed into quasi-isotropic (two-dimensionally isotropic) laminates. Each of the lamina is composed of either boron or carbon filaments placed unidirectionally in an epoxy matrix. Such a quasi-isotropic laminate has been shown to result in minimum weight (ref. 11) for the structures of the type considered in the present study. Because the laminate is two-dimensionally isotropic, it may be analyzed in the same manner as a metalic material. It remains only to find the equivalent composite properties to be used in the analysis.

Because the filament orientations must be dispersed in several directions to obtain isotropicity, the uniaxial stiffness of the composite will be reduced from that of the individual lamina. This reduction factor can be determined using the methods of reference 12. Let a quasi-isotropic laminate of total thickness T be in a state of plane stress in its plane of isotropicity. Then from (3-36)* the midplane stress resultant-strain relations are

$$N_x = A_{11}\,\varepsilon_x + A_{12}\,\varepsilon_y$$

$$N_y = A_{12}\,\varepsilon_x + A_{22}\,\varepsilon_y$$

where the xy plane is the plane of isotropicity. By analogy with isotropic materials we define the equivalent isotropic modulus of elasticity as

$$E_e = \frac{1}{T}\,A_{11} = \frac{1}{T}\,A_{22}$$

Let the laminate have n layers of equal thickness $t = \frac{T}{n}$. Then from (3-25)

$$A_{11} = \sum_{k=1}^{n} (\bar{Q}_{11})_k\,(h_k - h_{k-1}) = t \sum_{k=1}^{n} (\bar{Q}_{11})_k$$

*all equations refer to Ref. 12.

From (2-35), for each layer,

$$(\bar{Q}_{11})_k = Q_{11}\cos^4\theta_k + 2(Q_{12}+2Q_{66})\sin^2\theta_k\cos^2\theta_k + Q_{22}\sin^4\theta_k$$

where θ_k is the orientation of the filaments in the kth lamina and where, from (2-28),

$$Q_{11} = \frac{E_{11}}{1 - \nu_{12}\nu_{21}}$$

$$Q_{22} = \frac{E_{22}}{1 - \nu_{12}\nu_{21}}$$

$$Q_{12} = \frac{\nu_{12}\, E_{22}}{1 - \nu_{12}\nu_{21}}$$

$$Q_{66} = G_{12}$$

The five elastic constants which characterize the material are E_{11}, E_{22}, ν_{12}, ν_{21} and G_{12}, four of which are independent.

To impose isotropicity, we consider the limit of an infinite number of unidirectional bundles of fibers at equally spaced directions. Let j be the number of bundles having orientations between θ and $\theta + d\theta$ and let m be the number of increments $d\theta$. Then $mj = n$ and $j\pi = nd\theta$ so that

$$A_{11} = T \lim_{m\to\infty} \left\{ \frac{\sum_{k=1}^{m} j\,[\bar{Q}_{11}(\theta)]_k}{n} \right\}$$

$$= \lim_{\substack{m\to\infty \\ md\theta = \pi}} \left[\frac{T}{\pi} \sum_{k=1}^{m} [\bar{Q}_{11}(\theta)]_k\, d\theta \right]$$

$$= \frac{2T}{\pi} \int_0^{\pi/2} \bar{Q}_{11}(\theta)\, d\theta$$

Carrying out the integration

$$A_{11} = T\left[\frac{3}{8} Q_{11} + \frac{1}{4} (Q_{12} + 2Q_{66}) + \frac{3}{8} Q_{22}\right]$$

Since a bundle of fibers will have no transverse or shear stiffness,

$$Q_{11} = E_{11}, \; Q_{22} = Q_{12} = Q_{66} = 0$$

so that

$$E_e = \frac{3}{8} E_{11}$$

Applying the rule of mixtures (ref. 13 shows this to be a good approximation) gives the stiffness of the composite as

$$E_C = \frac{3}{8} E_{11_F} V_F + E_M (1 - V_F)$$

where V_F is the volume fraction of the filament. This expression was used in reference 14 and is used in this paper.

There are other candidate expressions for E_C and some of these will be briefly mentioned. In the first, the limit of an infinite number of orthotropic lamina is considered instead of fiber bundles. In this case, transverse and shear properties cannot be neglected with the result that

$$E_e = \frac{1}{T} A_{11} = \frac{3}{8} \frac{E_{11}}{1-\nu_{12}\nu_{21}} + \frac{(3+2\nu_{12})}{8} \frac{E_{22}}{1-\nu_{12}\nu_{21}} + \frac{1}{2} G_{12}$$

Using the approximations (ref. 15)

$$1 - \nu_{12}\nu_{21} = 1, \; \nu_{12} = 1/4, \; G_{12} = \frac{3}{8} E_{22}$$

results in

$$E_e = \frac{3}{8} E_{11} + \frac{5}{8} E_{22}$$

Applying the rule of mixtures to E_{11}

$$E_C' = \frac{3}{8} [E_{11_F} V_F + E_M (1-V_F)] + \frac{5}{8} E_{22}$$

where E_{22} depends on E_{22_F}, E_M and V_F and may be determined from reference 13 or 16.

Other expressions for E_C are obtained by considering the quasi-isotropic laminate subjected to axial loading. Then

$$N_x = A_{11}\,\varepsilon_x + A_{12}\,\varepsilon_y$$

$$0 = A_{12}\,\varepsilon_x + A_{22}\,\varepsilon_y$$

or

$$N_x = \left(A_{11} - \frac{A_{12}^2}{A_{22}}\right)\,\varepsilon_x$$

and we take the equivalent isotropic stiffness as

$$E_e = \frac{1}{T}\,(A_{11} - A_{12}^2/A_{22})$$

In the same manner as for A_{11}, the following are obtained

$$A_{22} = A_{11} = T\left[\frac{3}{8}\,Q_{11} + \frac{1}{4}\,(Q_{12} + 2Q_{66}) + \frac{3}{8}\,Q_{22}\right]$$

$$A_{12} = T\left[\frac{1}{8}\,(Q_{11} + Q_{22}) - \frac{1}{2}\,Q_{66} + \frac{3}{4}\,Q_{12}\right]$$

If bundles of fibers are considered and the transverse and shear stiffnesses are neglected, there results

$$E_e = \frac{1}{3}\,E_{11}$$

Applying the rule of mixtures gives

$$E_C'' = \frac{1}{3}\,E_{11_F}\,V_F + E_M\,(1-V_F)$$

If, on the other hand, layers of lamina are considered and the same approximations ar used as for E_C', there results

$$E_C''' = \frac{(\frac{3}{8} E_{11} + \frac{5}{8} E_{22})^2 - (\frac{1}{8} E_{11} + \frac{1}{8} E_{22})^2}{\frac{3}{8} E_{11} + \frac{5}{8} E_{22}}$$

where

$$E_{11} = E_{11_F} V_F + E_M (1-V_F)$$

Calculations show that the various expressions for E_C differ by about 10% for B/E and 3% for C/E. Since values of E_{22} must be determined experimentally, it was decided not to use methods employing this quantity.

For the composite density, the rule of mixtures is used

$$\rho_C = \rho_F V_F + \rho_M (1 - V_F)$$

It is assumed that composite strength is reduced by the same relative amount as the stiffness (ref. 11); thus

$$F_C = \frac{3}{8} F_F V_F + F_M (1 - V_F)$$

The properties of both the composite constituents and the composites themselves (with $V_F = 0.5$) are shown in Table C1. Also shown are the properties of the aluminum alloy used in the study. Since the weight of buckling critical structure is approximately proportional to the quotient $\rho\sqrt{E}$, this value is also given in the table, relative to aluminum.

APPENDIX D - LIFT AND DRAG ANALYSIS

Lift Characteristics

The lift characteristics, in terms of C_{L_α}, were calculated using a thin-wing paneling program developed by Ralph Carmichael at the Ames Research Center and based on the theory of reference 17. The analysis uses the method of aerodynamic influence coefficients, whereby the wing is divided into many small regions or panels with swept leading and trailing edges to conform to the actual wing geometry. Bilateral symmetry is assumed for all wings. The lifting pressure difference is assumed to be constant over each wing panel. The number of panels into which the wing is divided affects both the accuracy and the computer time required for the solution. As expected, the error decreases with increasing number of panels, although the convergence is rather slow. From a practical point of view, it is fortunate that answers with adequate accuracy for engineering analysis can be obtained with a relatively small number of panels, say 20-40. Since the computing time is roughly proportional to the square of the number of panels, the use of a fine grid is justified only when a high degree of accuracy is required. In the analysis of cambered and twisted wings, however, it is usually necessary to use a large number of panels in order to adequately describe the wing camber surface. Since, in the use of this program for the analysis of advanced commercial transport configurations, it is currently not necessary to consider camber and twist, the wing lift characteristics can be adequately estimated with thirty-six panels.

Zero-Lift Drag

The zero-lift drag (C_{D_0}), for each configuration was estimated by adding the friction drag of the wing, fuselage, horizontal, and vertical tail, together with any applicable wave drag. The nacelle friction drag was included in the engine performance calculation. For configurations designed to cruise at speeds less than Mach 1, no wave drag was included. Also, no separation drag component was included in the zero-lift drag estimate. The estimated wing separation drag was included in the calculation of induced drag, as will be discussed subsequently.

The friction drags for the aircraft components were computed using the following relations:

The wing friction drag was estimated based on turbulent boundary layer, flat-plate skin friction and contains an empirical correction for thickness induced pressure fields. The basic equation is Frankl and Voishel's extension of Von Karman's mixing-length hypothesis to compressible flow, and the empirical correction for thickness-induced pressure fields is the result of a correlation in reference 18 of a large amount of data. The resulting equation is as follows:

$$C_{D_{FW}} = 0.455 \frac{\left[1 + 2\left(\frac{t}{c}\right)_{wing}\right]\left(\frac{S_{WET}}{S_{REF}}\right)}{(\log_{10} Re)^{2.58}\left(1 + \frac{\gamma - 1}{2} M^2\right)^{0.467}}$$

where,

$\left(\frac{t}{c}\right)_{wing}$ = wing thickness ratio

S_{WET} = wing wetted area, not including portion of wing buried in the fuselage, ft^2

S_{REF} = reference area, idealized wing planform area, ft^2

Re = Reynold's Number based on the wing mean-aerodynamic-chord

γ = ratio of specific heats for air

M = Mach number

The fuselage friction drag was estimated with the same equation as used for the wing friction drag. However, the correction for thickness induced pressure fields is changed to the correct form for axisymmetric bodies:

$[1 + 2 (\frac{t}{c})_{wing}]$ is replaced by

$[1 + \frac{1}{2} (\frac{1}{d})_{BODY}]$

where, $(\frac{1}{d})_{BODY}$ = fuselage fineness ratio

Also, for the fuselage friction drag the Reynold's Number used in the equation is based on body length and S_{WET} is the fuselage wetted area.

The horizontal and vertical tail friction drags were estimated with the same equation as used for the wing friction drag. In this case, the Reynold's Number is based on the appropriate mean-aerodynamic-chord and the thickness ration and wetted area used are those of the particular surface.

No wave drag was included for the CVT configuration, which was designed to cruise at Mach 0.90. It was assumed that wave drag of the CVT with the supercritical wing would be negligible. Also, for the ATT configuration, which was designed to cruise at Mach 0.98, no wave drag was included. For

the ATT it was assumed that any wave drag would be negligible because of the supercritical wing and fuselage area ruling.

The wave drag of the TST configuration, which was designed to cruise at Mach 1.15, was estimated as the theoretical wave drag of a axisymmetric body with a Sears-Haack area distribution plus the wave drag of the horizontal and vertical tails, without any interference drag.

The wave drag of a body with a Sears-Haack area distribution is the theoretical minimum for an axisymmetric body of a given length and volume. The form of the equation used for the Sears-Haack wave drag computation is as follows (ref. 19):

$$C_{D_{WB}} = 14.6 \frac{(VOL_{SH})^{2/3}}{\left(\frac{l_{SH}}{d_{SH}}\right)^{8/3} S_{REF}}$$

where, $VOL_{SH} = \frac{3}{64} \pi^2 l_{SH} d_{SH}^2$

VOL_{SH} = volume of the Sears-Haack area distribution, ft^3

l_{SH} = length of the Sears-Haack area distribution, ft

d_{SH} = maximum diameter of the Sears-Haack area distribution, ft

The equations used for estimating the wave drag of the horizontal and vertical tails are for values at Mach 1.0 and the Mach number for shock attachment at the fin leading edge. The value used at Mach 1.15 was obtained by linear interpolation between these two values. The equations for both fins are of the same form. Using the appropriate values of thickness ratio, exposed area, and sweep for that fin, the equations are as follows (ref. 20):

At $M = 1.0$, $C_{D_{WF}} = 3.4 \left(\frac{t}{c}\right)^{5/3}_{fin} \frac{S_{fin}}{S_{ref}} \cos^2 \Lambda_{fin}$

At $M =$ secant Λ_{fin},

$$C_{D_{WF}} = 6 \left(\frac{t}{c}\right)^{2}_{fin} \frac{1}{\beta} \frac{S_{fin}}{S_{ref}}$$

where, $\left(\frac{t}{c}\right)_{fin}$ = fin fineness ratio

S_{fin} = fin exposed planform area, ft^2

Λ_{fin} = fin leading edge sweep, deg

β = compressibility factor $(|M^2 - 1|)^{1/2}$

Induced Drag

The induced drag of all configurations was estimated using an equation made up of the sum of three components: vortex drag, wave drag, and separation drag. The induced drag level is related to a parameter called $K_{C_{D_i}}$ defined by

$$K_{C_{D_i}} = \frac{C_{D_i}}{C_L^2/\pi AR}$$

where C_{D_i} = induced drag coefficient and $C_L^2/\pi AR$ is the theoretical minimum subsonic induced drag, with Oswald's efficiency factor equal to 1.

The vortex drag was estimated to reduce Oswald's efficiency factor from 1.0 to 0.85, which corresponds to a $K_{VC_{D_i}}$ (the K factor for vortex drag) of 1.18. The lift induced wave drag component was estimated at the theoretical minimum level given in references 21 and 22. This wave drag component was only included at speeds greater than Mach 1. The form of

this equation for conventional swept wings is as follows:

$$K_{wave} = K_w \frac{2\beta^2}{(\tan \Lambda_{LE} + \frac{\lambda}{1+\lambda} \frac{4}{A})^2}$$

where, K_w = 1.0, value for wing shapes of nearly elliptic loading both spanwise and lengthwise, as defined in reference 22.

Λ_{LE} = wing leading edge sweep, deg

λ = wing taper ratio, tip chord/centerline chord

AR = wing aspect ratio, span^2/wing area

The separation drag component was estimated from experimental data in reference 23. The separation drag estimate was included in an effort to realistically account for this drag component, which is difficult to compute theoretically.

Figure D1 shows a comparison of the theoretical estimate of induced drag without including separation drag with some experimental data from reference 23. Based on this experimental data an empirical relation for estimating separation drag was derived. The resulting equation is as follows:

$$K_{sep} = \left(\frac{C_L}{0.2}\right)^{3/2} (K_{vortex} + K_{wave} - 1.0)$$

where, C_L = lift coefficient

The expression for the induced drag coefficient resulting from combining the previously discussed components is as follows:

$$C_{D_i} = \frac{C_L^2}{\pi AR} [K_{vortex} + K_{wave} + K_{sep}]$$

The induced drag of aircraft designed to cruise in the transonic speed regime is one of the most challenging aerodynamic quantities to predict. Realizing possible weakness in the estimation technique presented here, we have included several optional methods in the aerodynamics program. These optional estimation methods range from ideal subsonic induced drag with full leading edge suction (Oswald's efficiency factor equal to 1) to supersonic induced drag, corresponding to no leading edge suction ($C_{D_i} = C_L \tan \alpha$). The sensitivity to the induced drag estimate resulting from these various methods is given in the text of this report.

APPENDIX E - AREA RULING

The area ruling program described herein was developed in response to the requirement for a simplified design tool to use as part of the TRANSYN-TST analysis of advanced technology transport aircraft. The purpose of the program is to calculate the fuselage cross-sectional area distribution which, when combined with the wing and nacelle area distributions, will result in a given overall equivalent area distribution (a Sears-Haack area distribution in this study). The program is restricted to normal cross-sectional cuts and only includes the cross-sectional areas of the fuselage, wing, and engine nacelles. The fuselage area distribution is required for use in the fuselage structural weight calculation. Fuselage structural weight is dependent on the amount of area ruling required because the area ruling results in decreases in the fuselage diameter in the region where the fuselage bending moments are high.

To maintain the same passengers capacity in an area-ruled fuselage as in an equivalent cylindrical fuselage, the floor area of each is made the same. This assumes that the efficiency of seat placement in an area-ruled configuration is the same as that for a cylindrical fuselage. Since this assumption is somewhat unrealistic, several area-ruled fuselages were examined to determine the actual number of seats that could be accommodated. Based on the results of this study, the floor area required for the area-ruled fuselage was increased slightly to allow for less efficient floor area utilization resulting from the varying fuselage diameter. For more detailed studies, it would be desirable to accurately compute the number of seats that could be accommodated for each fuselage area distribution. This would involve a station-by-station examination over the length of the fuselage.

In the TRANSYN-TST program, the area-ruling procedure is divided into several subroutines. These subroutines calculate the cross-sectional area distributions of the wing alone, of the engine nacelles (minus the flow-through area), and of the fuselage (allowing for the wing and nacelles). The area distribution of the tails is not included, but this area would be removed from the fuselage in region of low bending moment concentration, and this omission would have a very small effect on the calculated fuselage weight.

For the calculation of the wing cross-sectional area distribution, the wing is assumed to be a constant airfoil section with a constant thickness ratio across the wing span. The chordwise thickness distribution is specified by the thickness ratio (t/c) at 12 stations over the chord of the section. Between these stations the thickness is determined by straight line interpolation. The specification of the airfoil thickness distribution, combined with the geometric description of the wing planform (sweep and taper ratio), completely describes the thickness distribution of the wing. The wing cross-sectional area distribution is calculated at 11 equally spaced streamwise stations along the wing region of influence, from the leading edge of the wing centerline section to the trailing edge of the tip airfoil section. The cross-sectional area distributions for several wings of different sweeps and thickness ratios are shown in figure E1.

The geometry of the nacelles is determined by the propulsion system analysis (ref. 2) and assumes that the nacelle is axisymmetric. The nacelle exterior profile consists of a constant diameter engine section and circular arc radius calculated for tangency to the engine section while meeting the inlet and exit requirements. For the area distribution calculations, the

interior shape of the flow-thru area is specified by a conical surface from the inlet lip to the nozzle lip. The effects of any exhaust gas expansion after leaving the nozzle are neglected in the area-ruling calculation. The total cross-sectional area distribution for multiple engines is dependent on the engine placement, and several subroutines have been developed for different types of engine installations (4, 6, and 8 wing-mounted engines, and 4 aft fuselage-mounted engines).

When the engines are wing mounted the nacelle cross-section areas are computed for same streamwise stations as used in the wing area distribution calculation. The nacelle and wing cross-sectional area distributions are then combined directly when area ruling the fuselage. When the engines are mounted on the aft fuselage, the nacelle cross-sectional areas are computed at 11 equally spaced streamwise stations along the nacelle region of influence, and this nacelle area distribution is accounted for separately during the fuselage area ruling.

To calculate the area distribution of the fuselage, the configuration geometry in the vicinity of the intersection of the wing and fuselage must be determined. For a low wing, the location of the wing was specified such that the bottom of a non-area ruled fuselage of the desired area distribution coincided with the lowest point on the wing. To provide maximum headroom as the body was necked down, the centerline of the fuselage was allowed to rise in the region above the wing. This displacement of the fuselage centerline was constrained so that the top of the area-ruled fuselage was not higher than for the non-area ruled fuselage and the bottom of the fuselage remained in contact with the wing. The cross-sectional area of the combined wing and fuselage also includes the area of a fillet at the fuselage-wing junction.

The objecti.e of the fuselage area ruling calculations was to determine the diameter distribution (d_{ARB}) of the area-ruled body that results in a given total cross-sectional area distributio. In solving for this diameter distribution three limiting cases arise. For the case where the wing is completely included in the original body (shown in figure E2 as Case I), no fuselage modification is required and d_{ARB} is equal to d_{CB}, the original fuselage diameter. When the wing cross-sectional area is completely exterior to the fuselage (an aft cut, shown in figure E2 as Case II), the diameter of the area-ruled body d_{ARB} is calculated based on the original fuselage area minus the wing cross-sectional area. When the area-ruled fuselage is tangent to the wing surface the geometry is shown in figure E2 as Case III. All other fuselage-wing intersections require a solution of the general case. This is handled in the program by a numerical technique, iterating on d_{ARB} until the required equivalent cross-sectional area is obtained.

In order to maintain the required floor area for the area-ruled configuration, there is an additional iteration which adjusts the body length in order to obtain the required floor area. The currently used procedure for maintaining the correct fuselage capacity is shown schematically in figure E3. First, an input cylindrical body is sized on the basis of number of seats, seats abreast, seat pitch, seat width, number of aisles, and nose and afterbody fineness ratio (assuming Sears-Haack nose and afterbody area distributions). Second, the volume of this fuselage is calculated and a Sears-Haack body with the same length and volume is computed. Third, the fineness ratio of the Sears-Haack body is held constant while the fuselage is area ruled for the wing and nacelles and the body length is increased to maintain the same floor area.

	CVT 235,000 lb		ATT 250,000 lb		TST 400,000 lb	
	AL	C/E	AL	C/E	AL	C/E
FUSELAGE WEIGHT	35,700	22,600	40,300	26,200	61,500	35,100
REDUCTION, percent	—	36.7	—	35.0	—	42.9
WING WEIGHT	21,800	14,600	27,000	17,500	54,100	33,900
REDUCTION, percent	—	33.0	—	35.2	—	37.3
O.W.E.	130,100	109,900	138,500	114,800	236,300	189,900
REDUCTION, percent	—	15.5	—	17.1	—	19.6

Table 1. Potential of Advanced Composites

COVERS	WEBS	ϵ	e	ϵ_c	e_c	ϵ_w	K_{g_c}	K_{g_w}
UNSTIFF	TRUSS	2.25	0.556	3.62	3	0.605	1.000	0.407
UNSTIFF	UNFLANG	2.21	0.556	3.62	3	0.656	1.000	0.505
UNSTIFF	Z STIFF	2.05	0.556	3.62	3	0.911	1.000	0.405
TRUSS	TRUSS	2.44	0.600	1.108	2	0.605	0.546	0.407
TRUSS	UNFLANG	2.40	0.600	1.108	2	0.656	0.546	0.505
TRUSS	Z STIFF	2.25	0.600	1.108	2	0.911	0.546	0.405

Table B1. Structural Coefficients and Exponents

MATERIAL	ρ (lb/in^3)	E ($lb/in^2 \times 10^6$)	F ($lb/in^2 \times 10^3$)	$\rho/\sqrt{E}$ RELATIVE TO Al
Al (2014 - T6)	0.101	10.5	61	1.00
BORON	0.090	60.0	400	0.37
CARBON (THORNEL 50)	0.059	50.0	285	0.27
EPOXY	0.050	0.5	100	—
B/E ($V_F = 0.5$)	0.070	11.5	125	0.66
C/E ($V_F = 0.5$)	0.055	9.6	103	0.57

Table C1. Material Properties

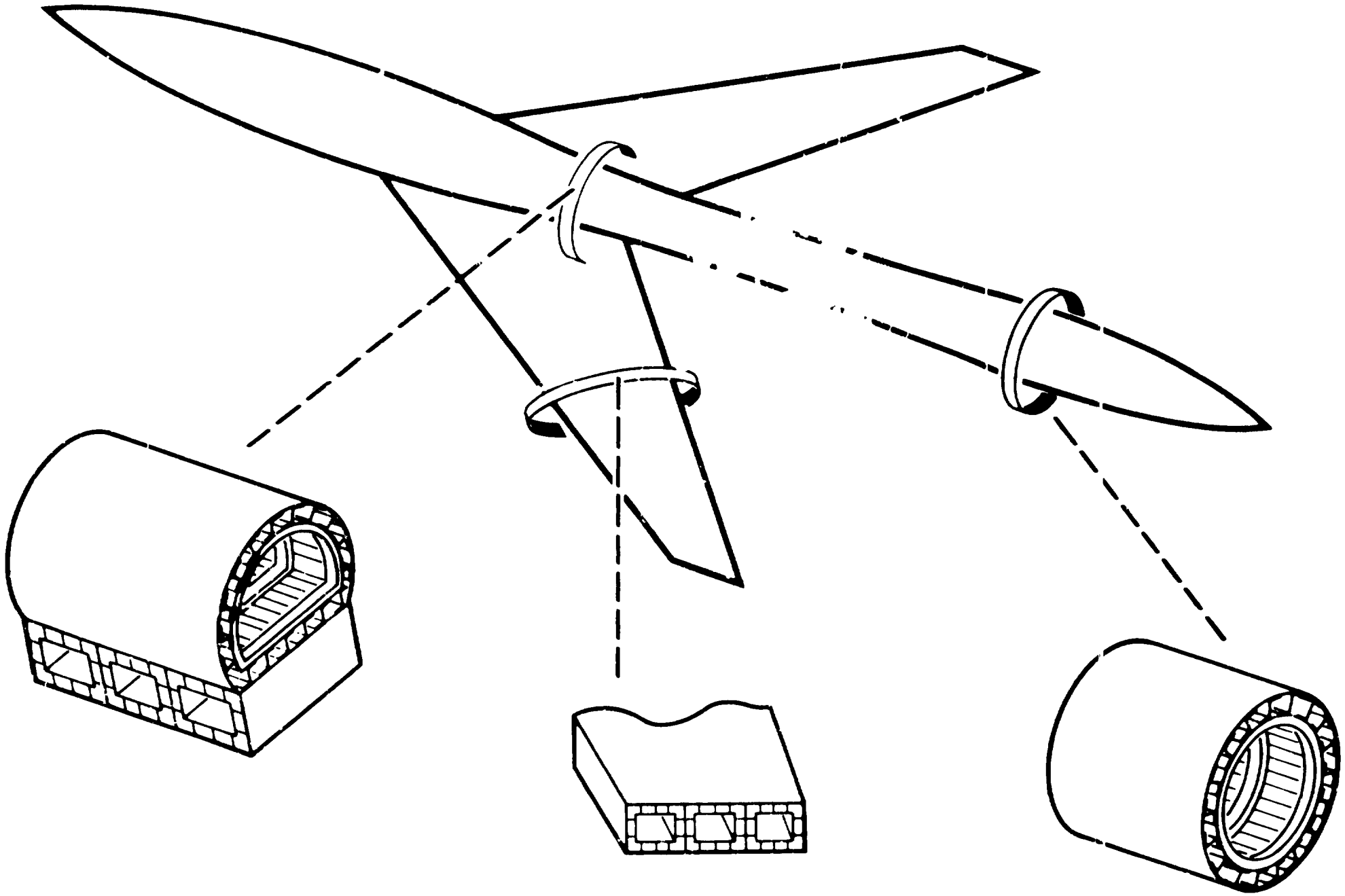

Figure 1. Structural Concepts

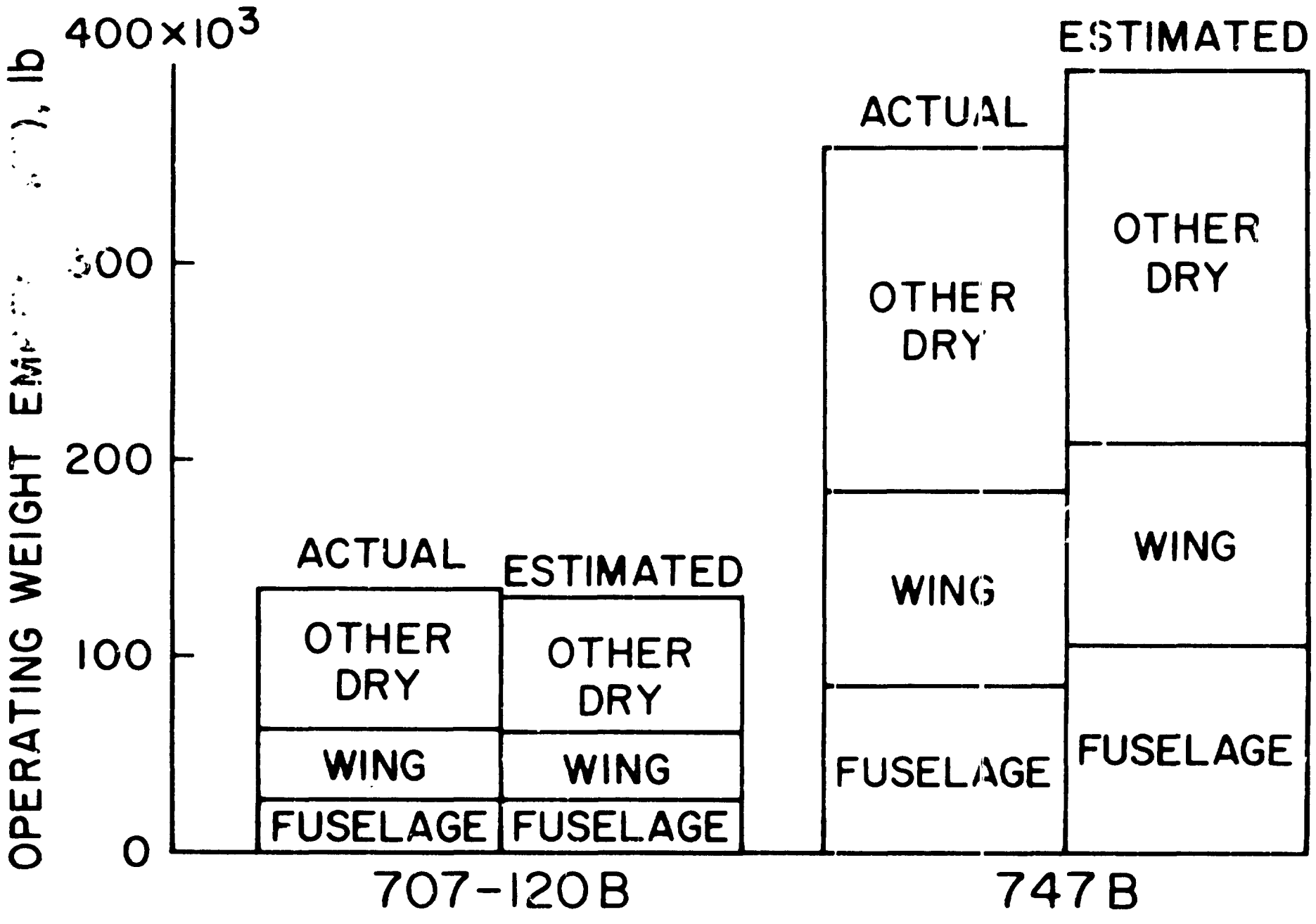

Figure 2. Comparison of Actual and Estimated Empty Weights

LIFT ~ C_{L_α} FROM AMES THIN WING PROGRAM

$C_{L_{MAX}}$ DOUBLE-SLOTTED FLAPS AND L.E. SLATS

DRAG ~ C_{D_F} SURFACE AREA FRICTION DRAG

C_{D_P} AREA RULE WAVE DRAG
(SEARS-HAACK AREA DISTRIBUTION)

C_{D_i} VORTEX DRAG WITH $e = 0.85$
+ MINIMUM WAVE DRAG
+ SEPARATION DRAG ESTIMATE

Figure 3. Aerodynamic Estimation Methods

CONFIGURATION	CVT	ATT	TST
CRUISE MACH NUMBER	0.90	0.98	1.15
WING SWEEP	35°	41°	50°
FUSELAGE AREA RULING	NO	YES	YES
WAVE DRAG PENALTY	NO	NO	YES

Figure 4. Major Differences Between Study Configurations

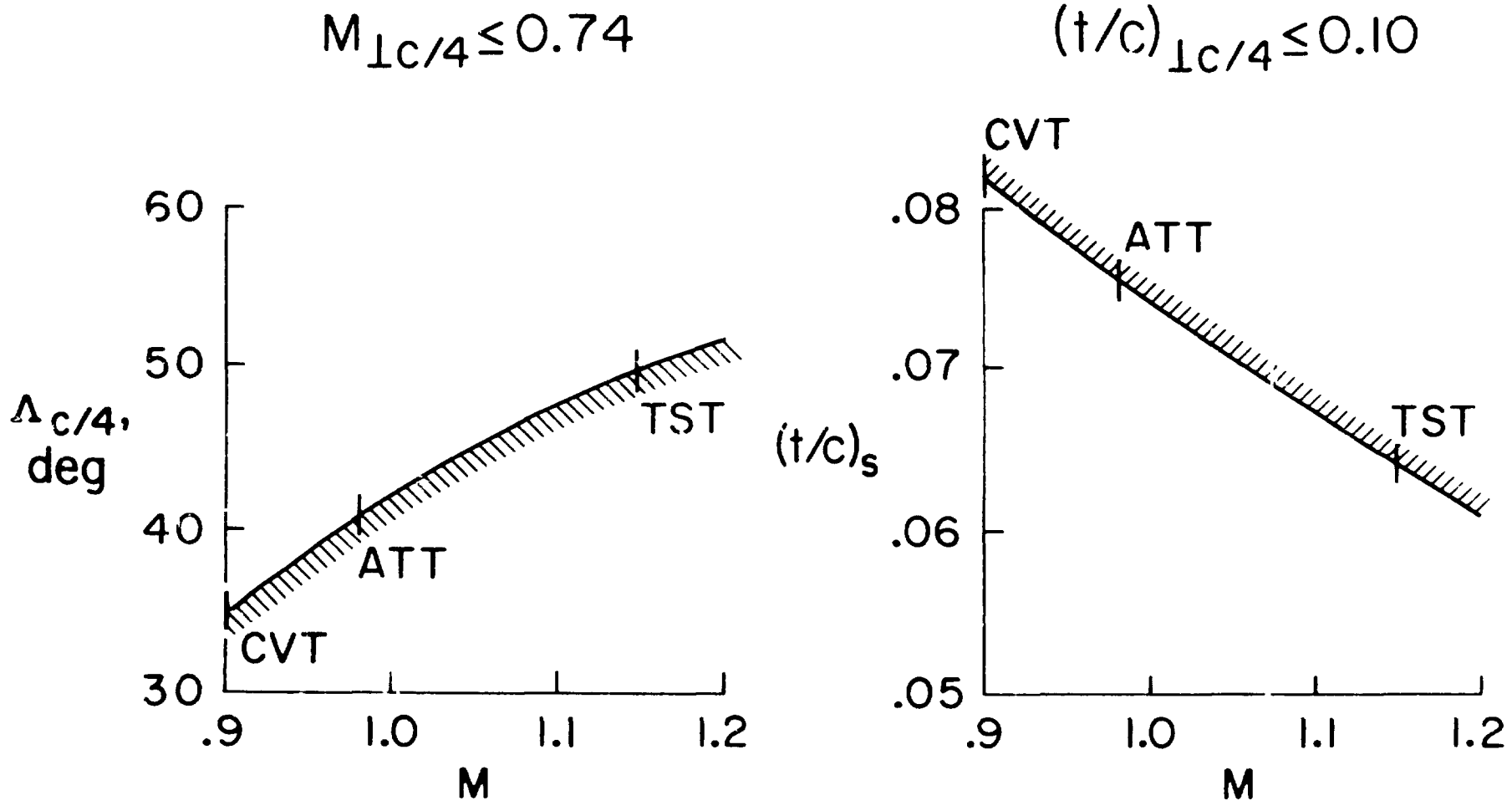

Figure 5. Aerodynamic Constraints

RANGE = 2700 n.mi. 200 PASSENGERS

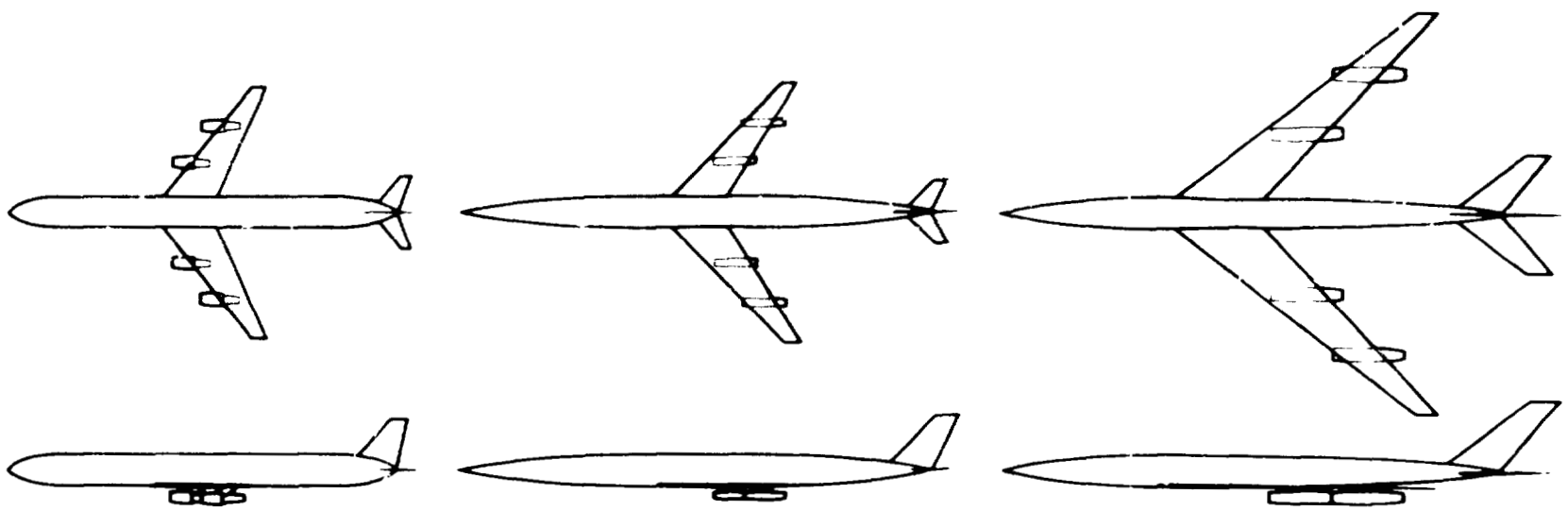

	CVT	ATT	TST
M_{CRUISE}	0.90	0.98	1.15
GROSS WEIGHT	235,000 lb	250,000 lb	600,000 lb
SWEEP (Λ)	35 deg	41 deg	50 deg
ASPECT RATIO (AR)	7	7	7
WING LOADING (w/s)	120 lb/ft^2	120 lb/ft^2	120 lb/ft^2

Figure 6. Nominal Configurations

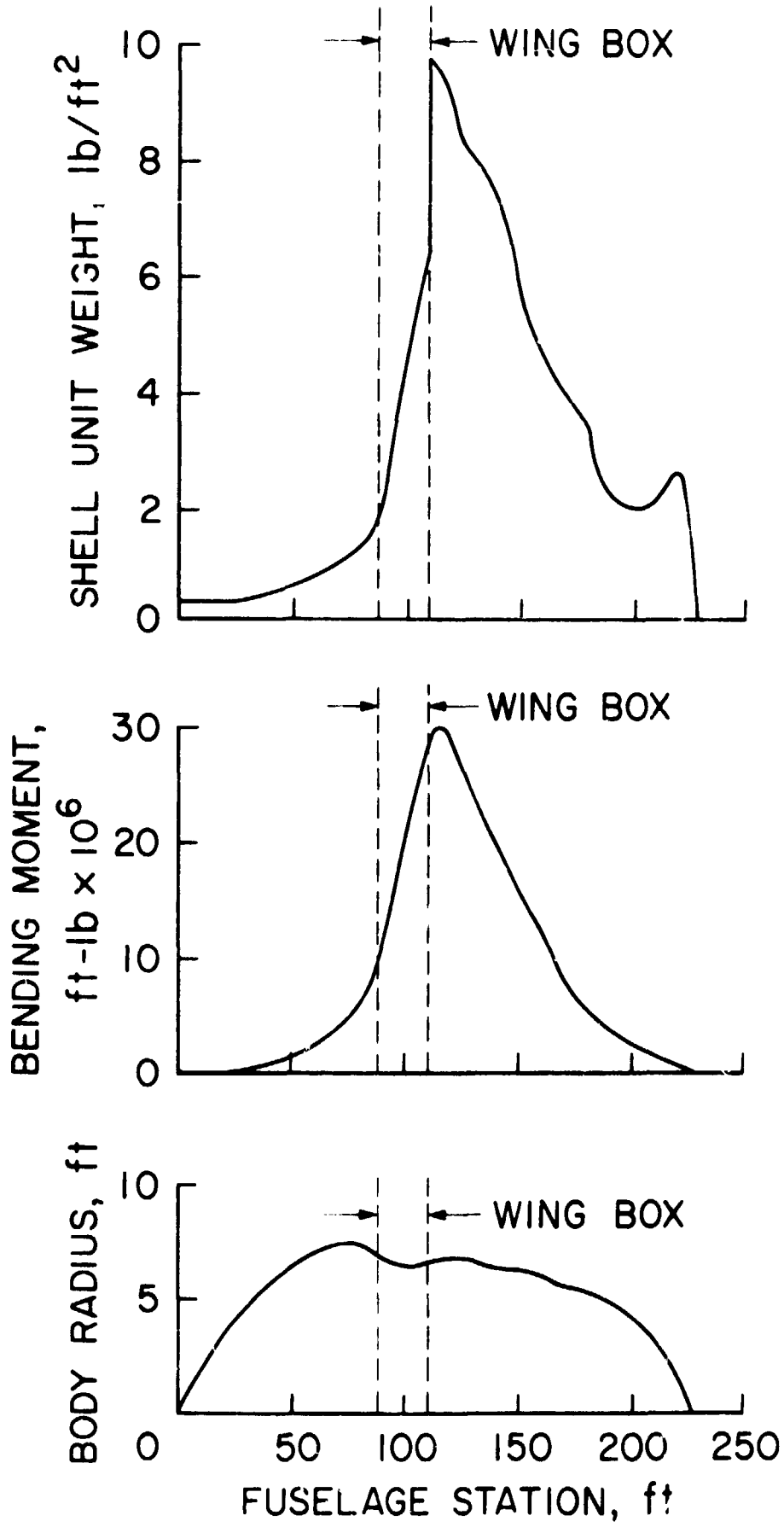

Figure 7. Body Weight Characteristics

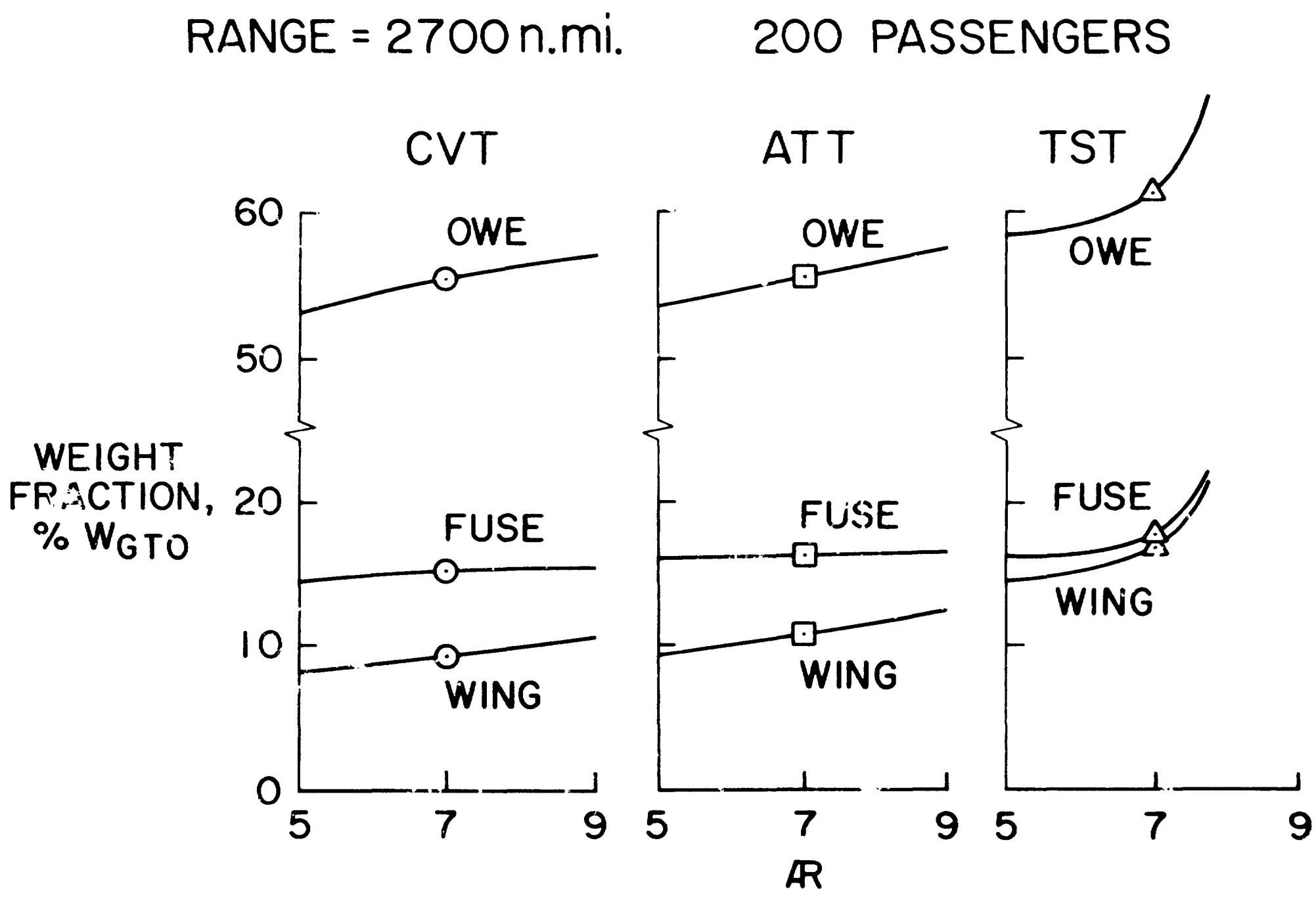

Figure 8a. Effect of Aspect Ratio on Weight Fractions

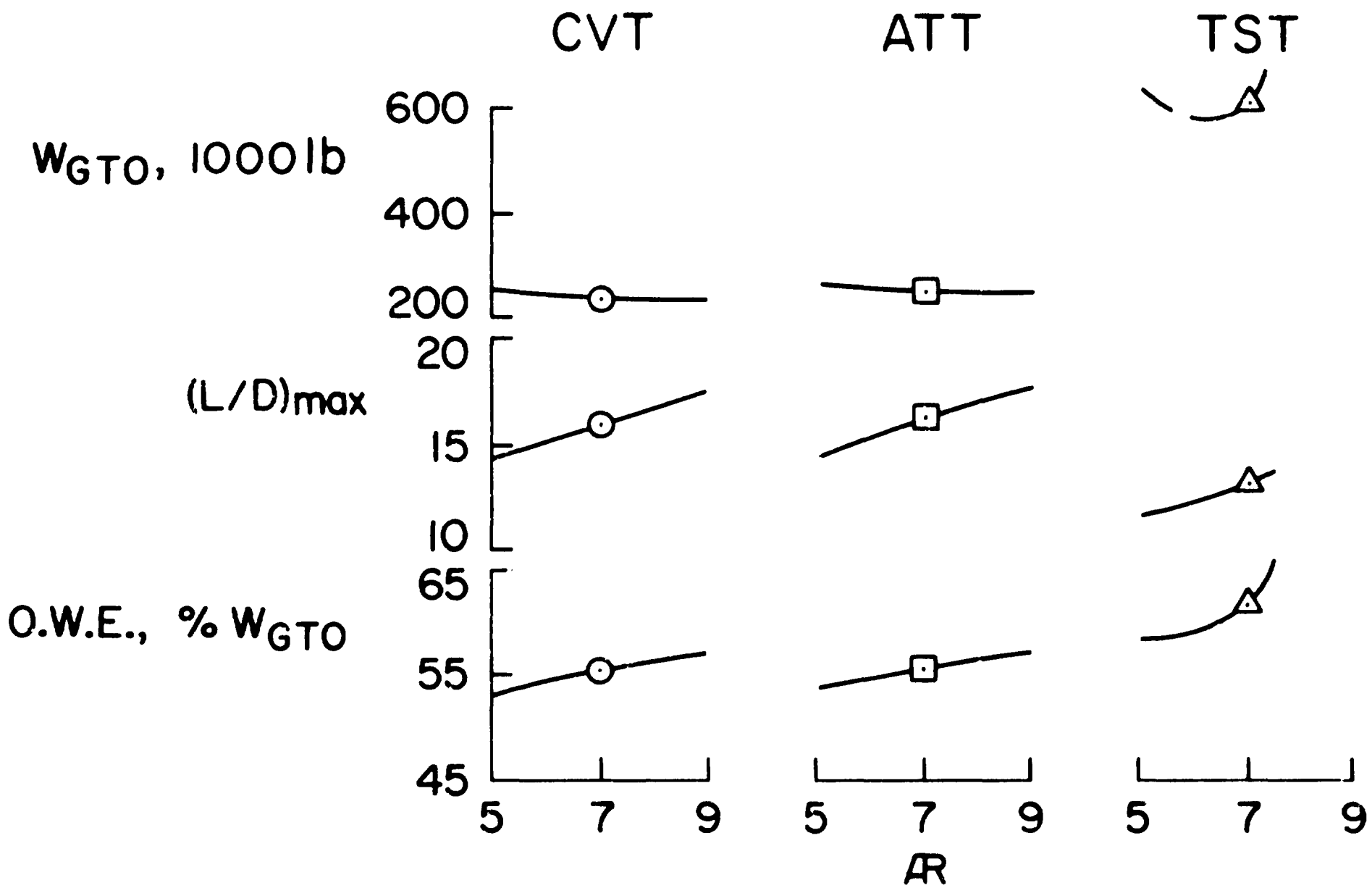

Figure 8b. Effect of Aspect Ratio on O.W.E., L/D_{max} and Gross Weight

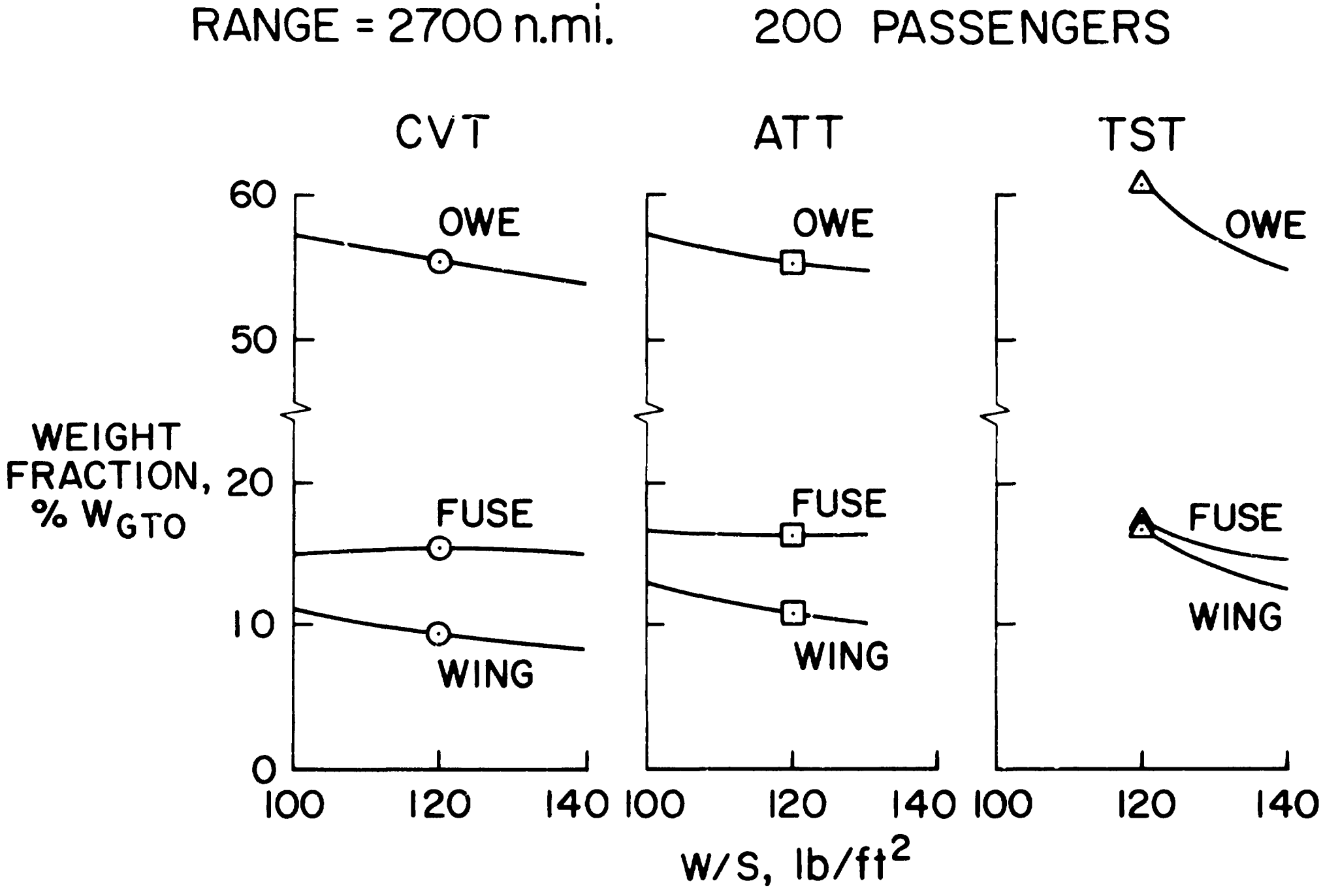

Figure 9a. Effect of Wing Loading on Weight Fractions

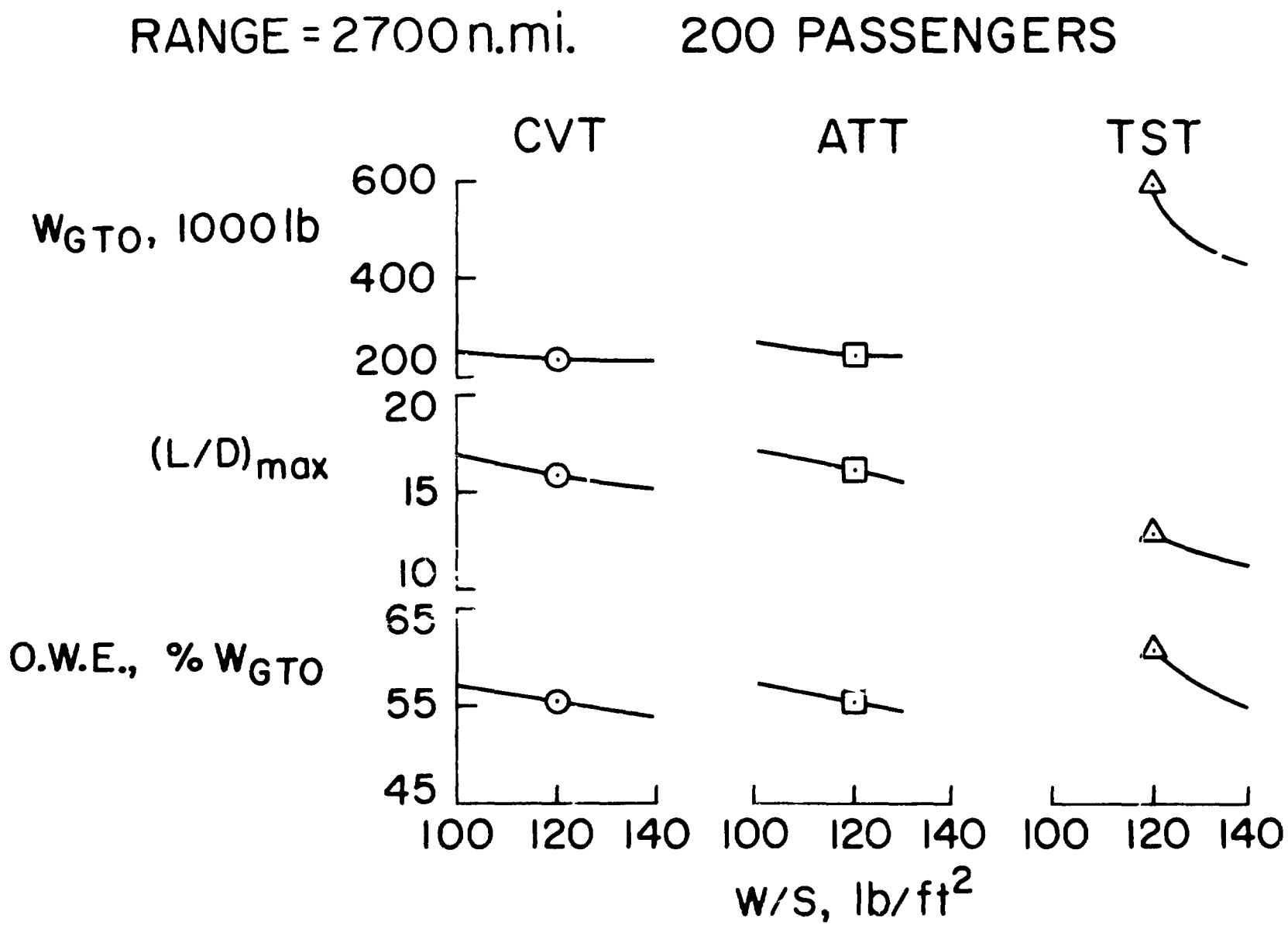

Figure 9b. Effect of Wing Loading on O.W.E., L/D_{max} and Gross Weight

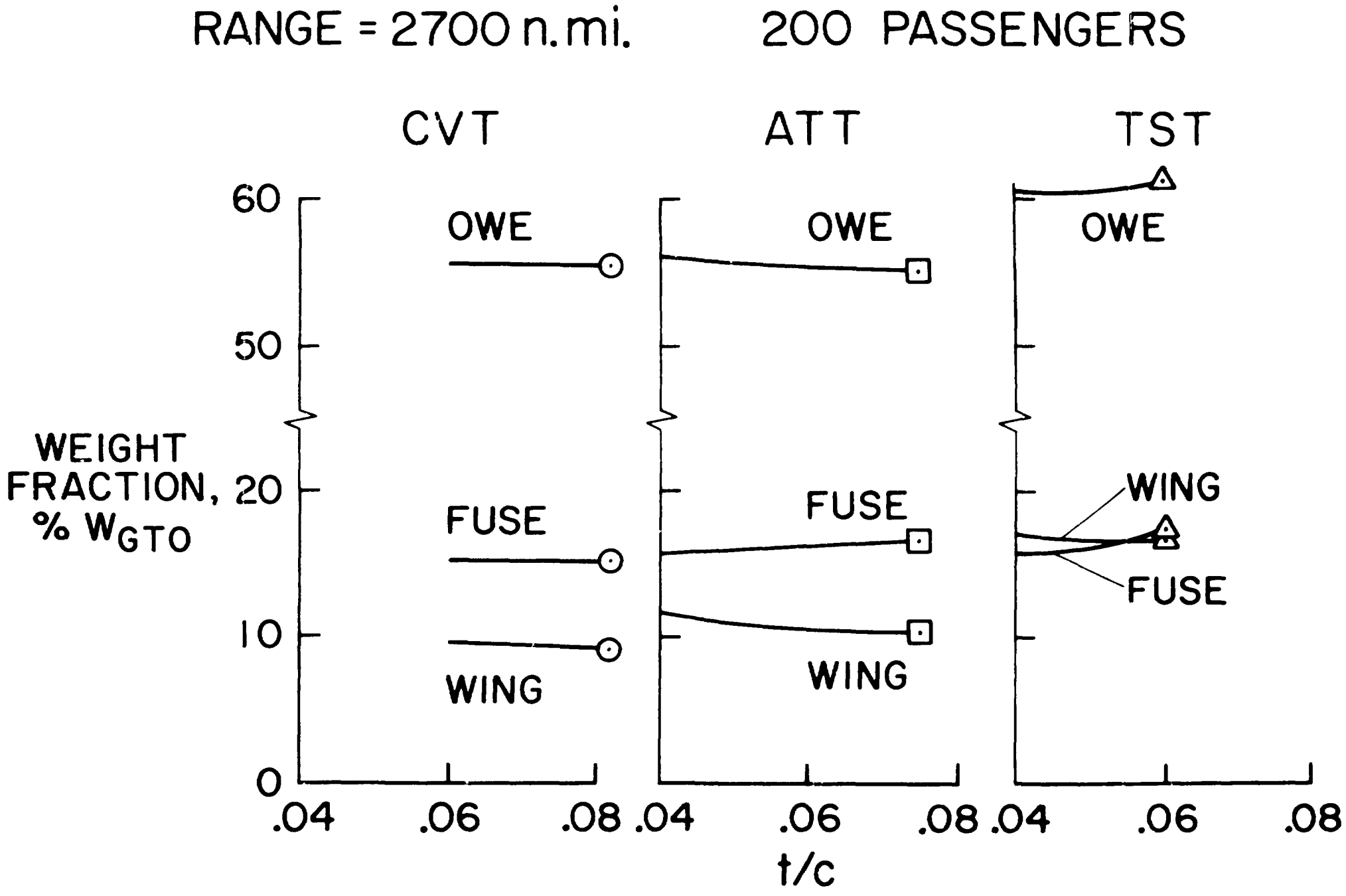

Figure 10a. Effect of Thickness-to-Chord on Weight Fractions

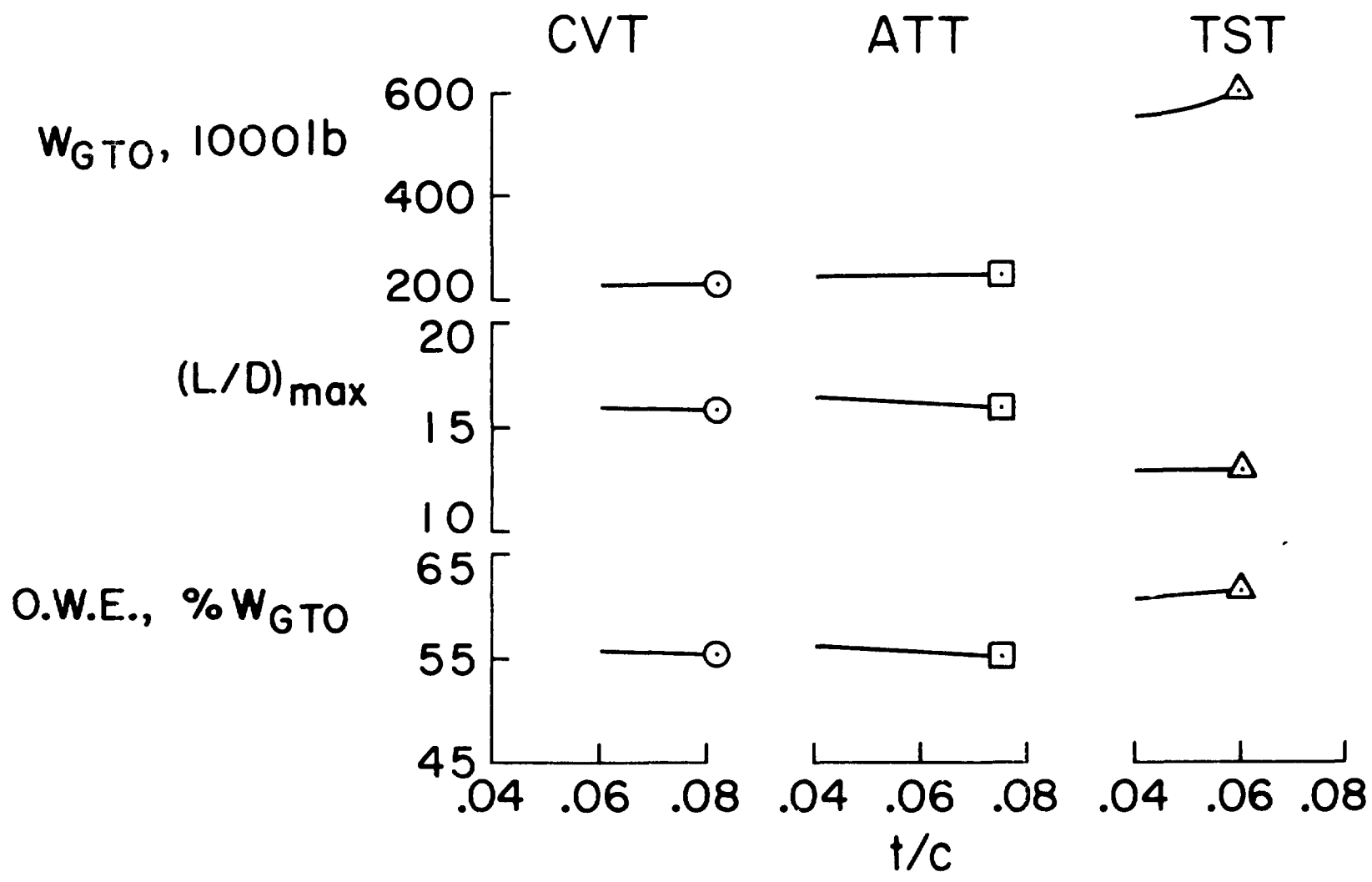

Figure 10b. Effect of Thickness-to-Chord on O.W.E., L/D_{max} and Gross Weight

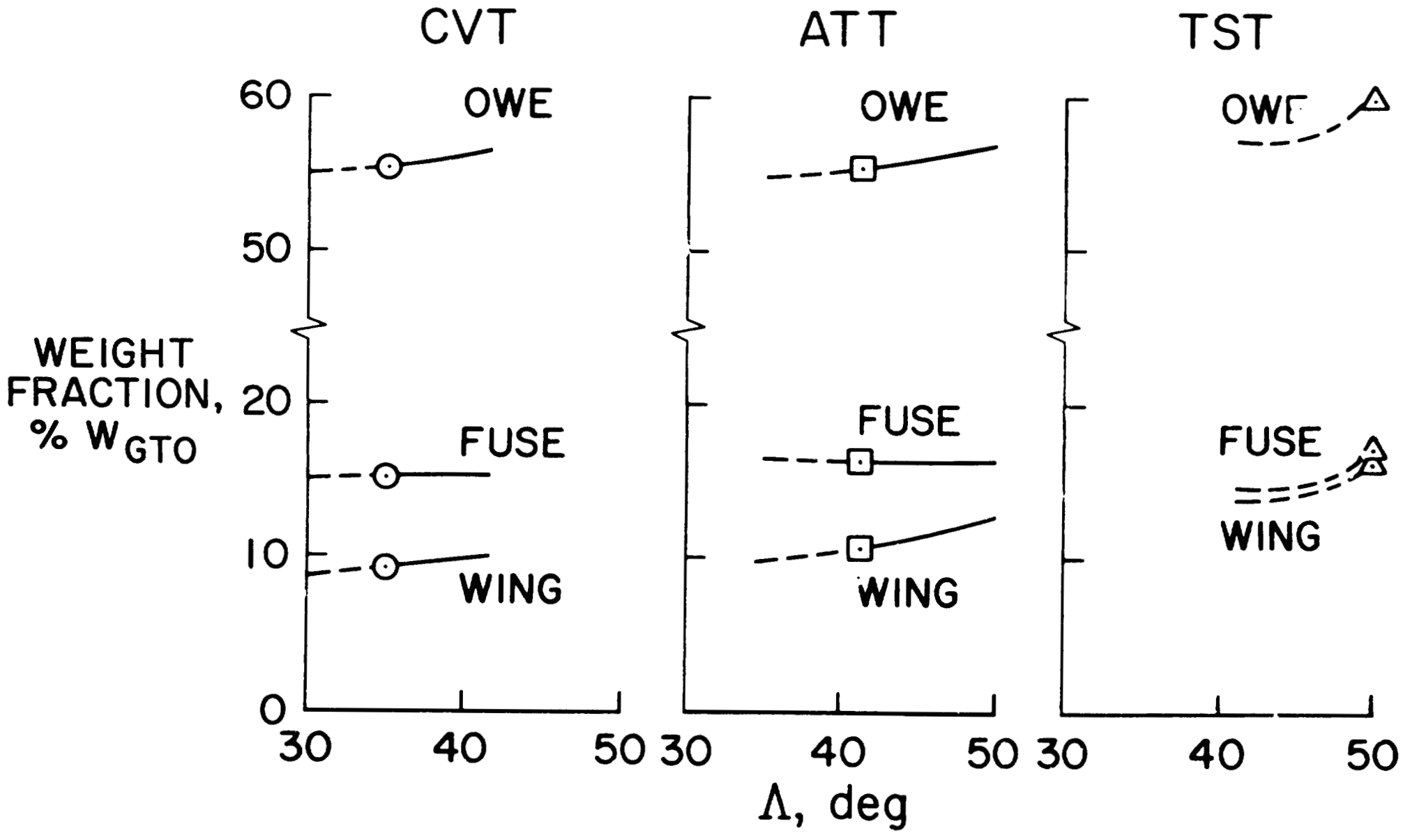

Figure 11a. Effect of Sweep on Weight Fractions

RANGE = 2700 n.mi. 200 PASSENGERS

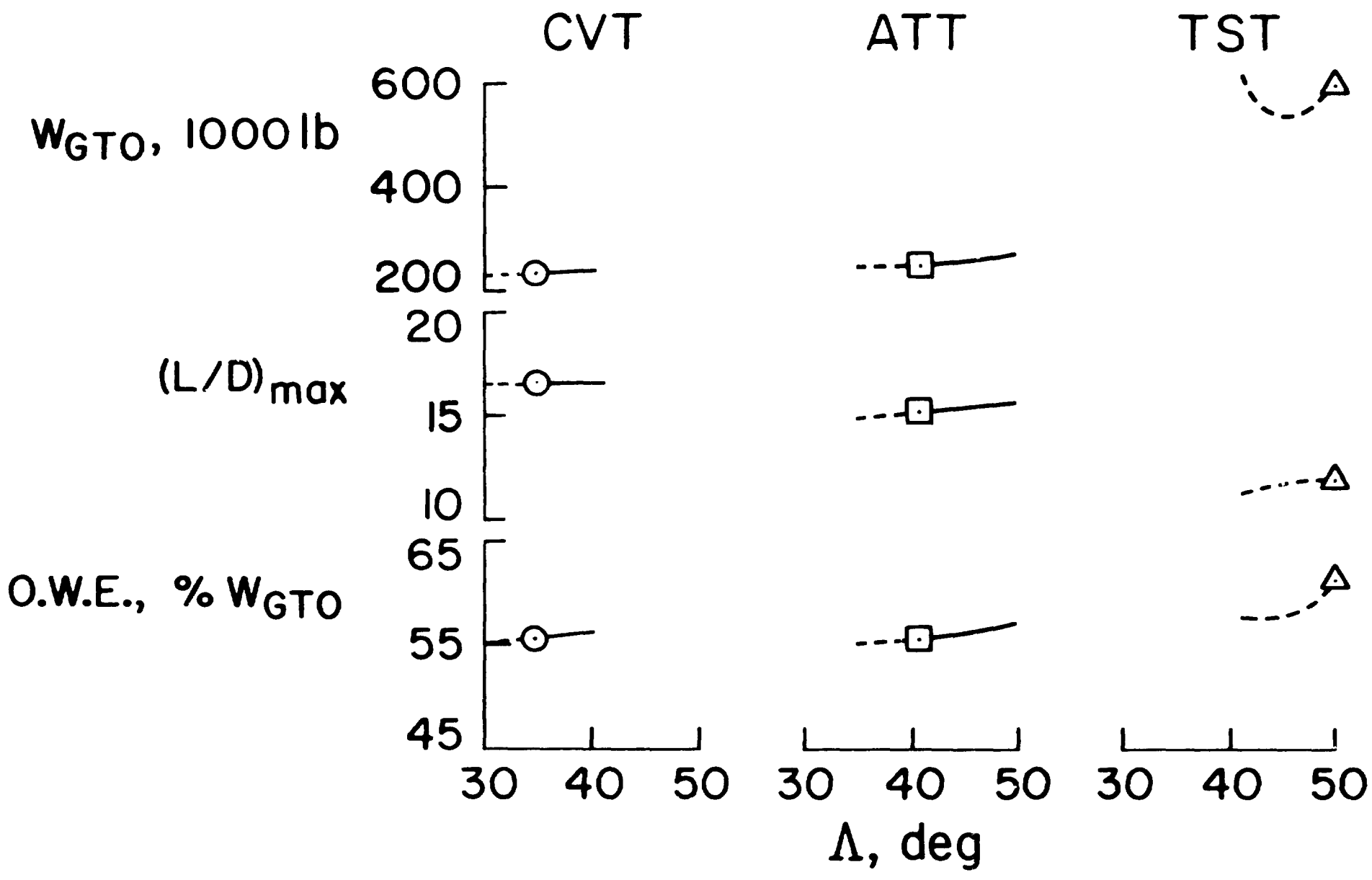

Figure 11b. Effect of Sweep on O.W.E., L/D_{max} and Gross Weight

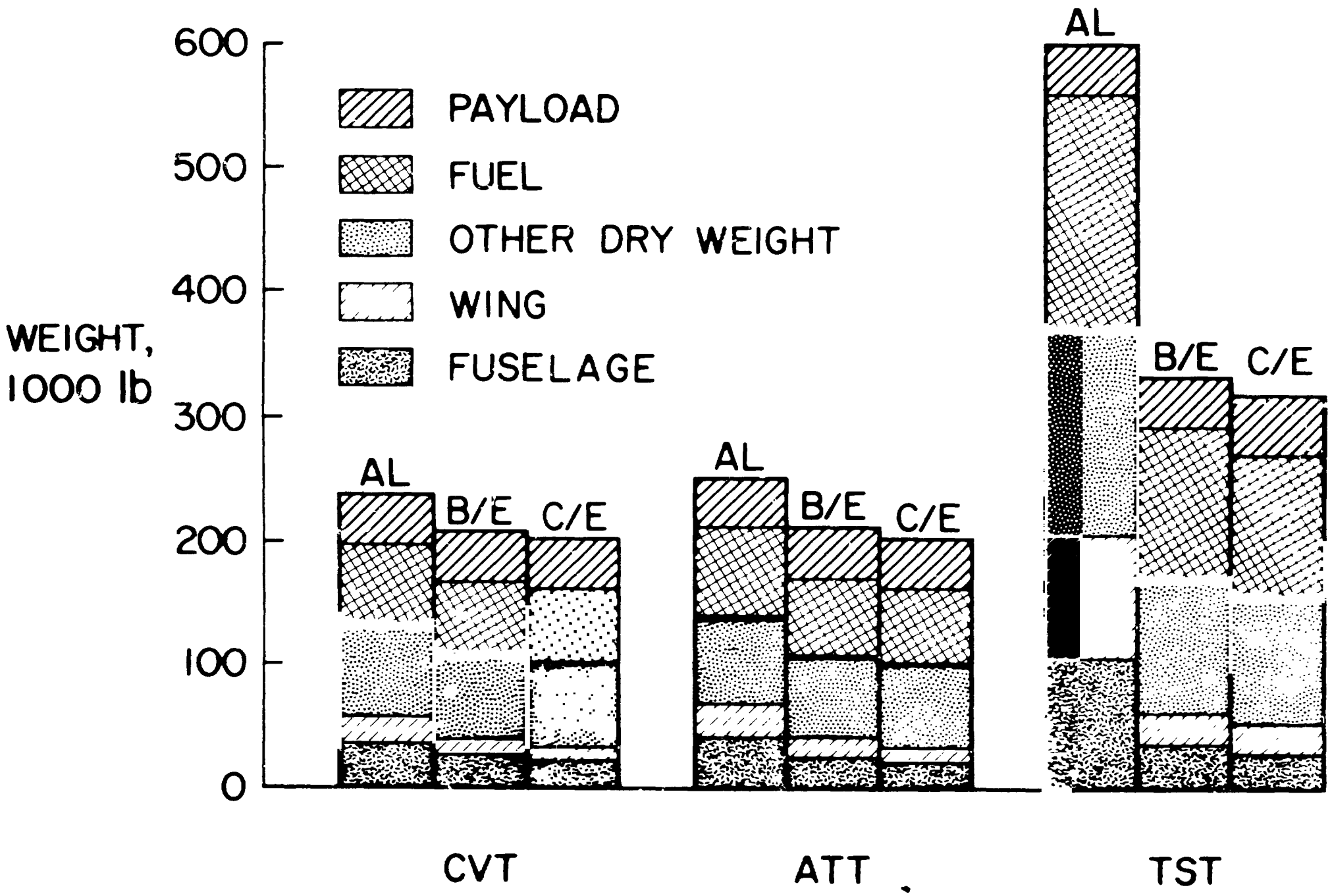

Figure 12. Weights of Nominal Configurations

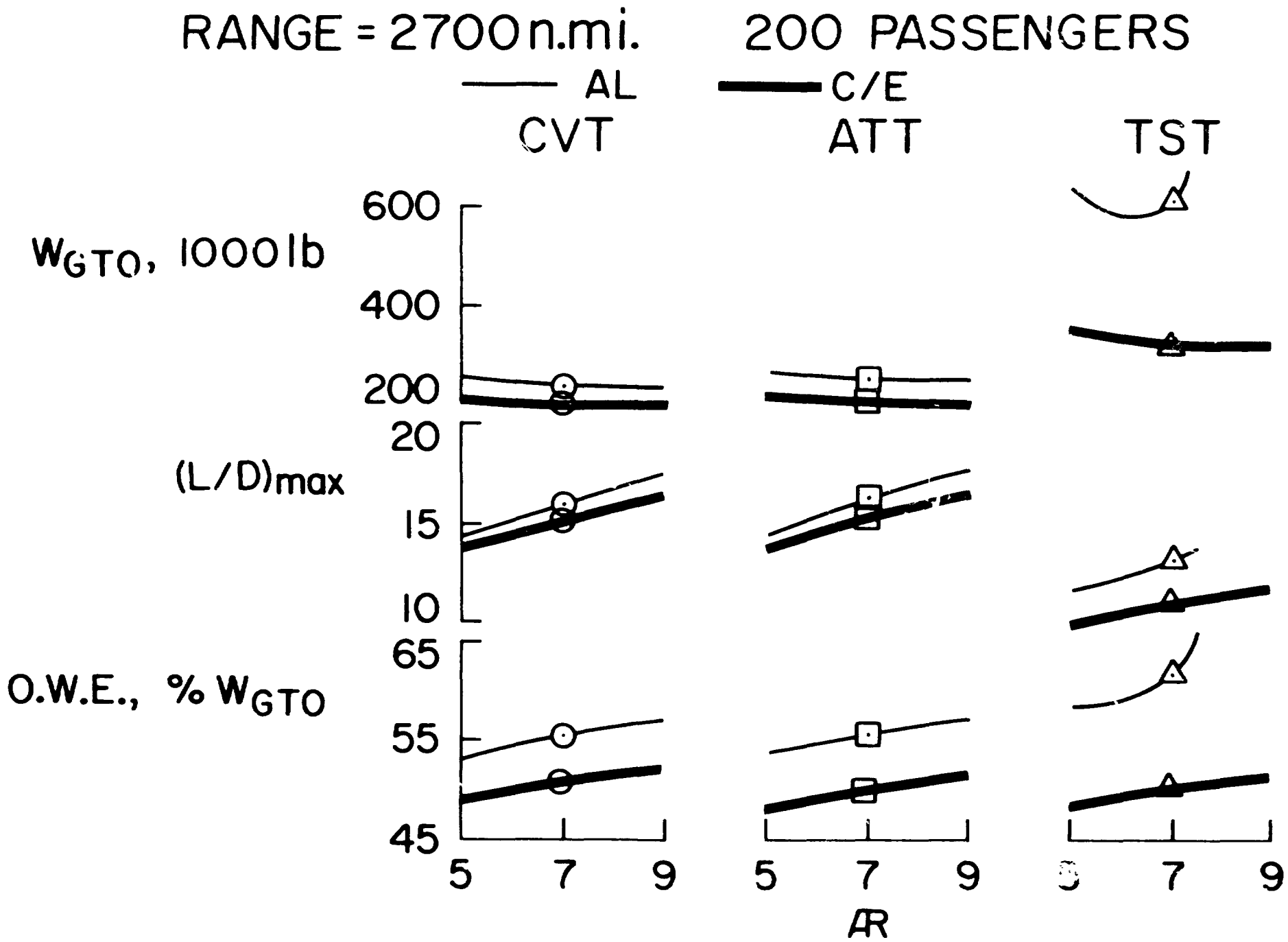

Figure 13. Effect of Aspect Ratio on O.W.E., L/D_{max} and Gross Weight

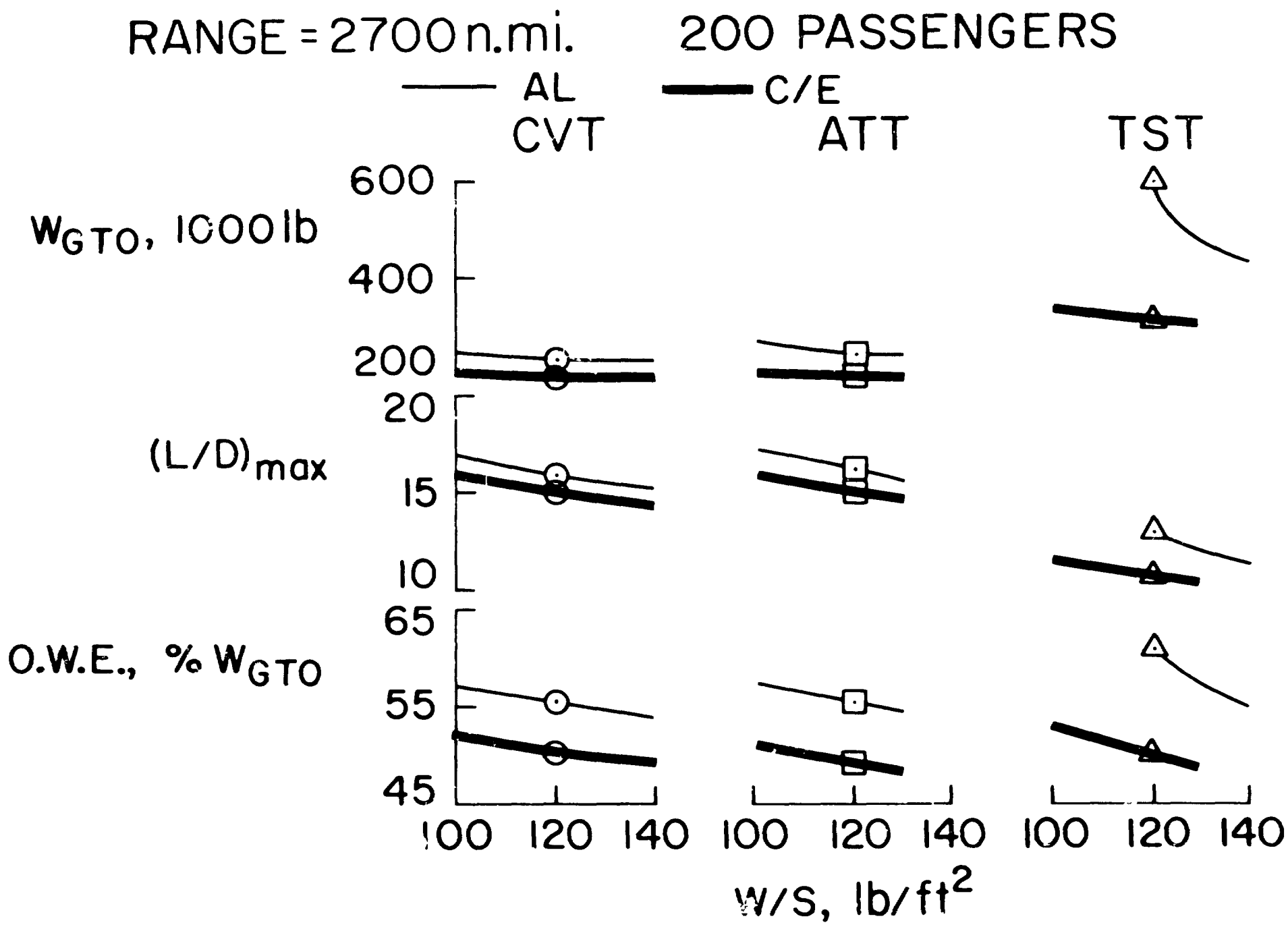

Figure 14. Effect of Wing Loading on O.W.E., L/D_{max} and Gross Weight

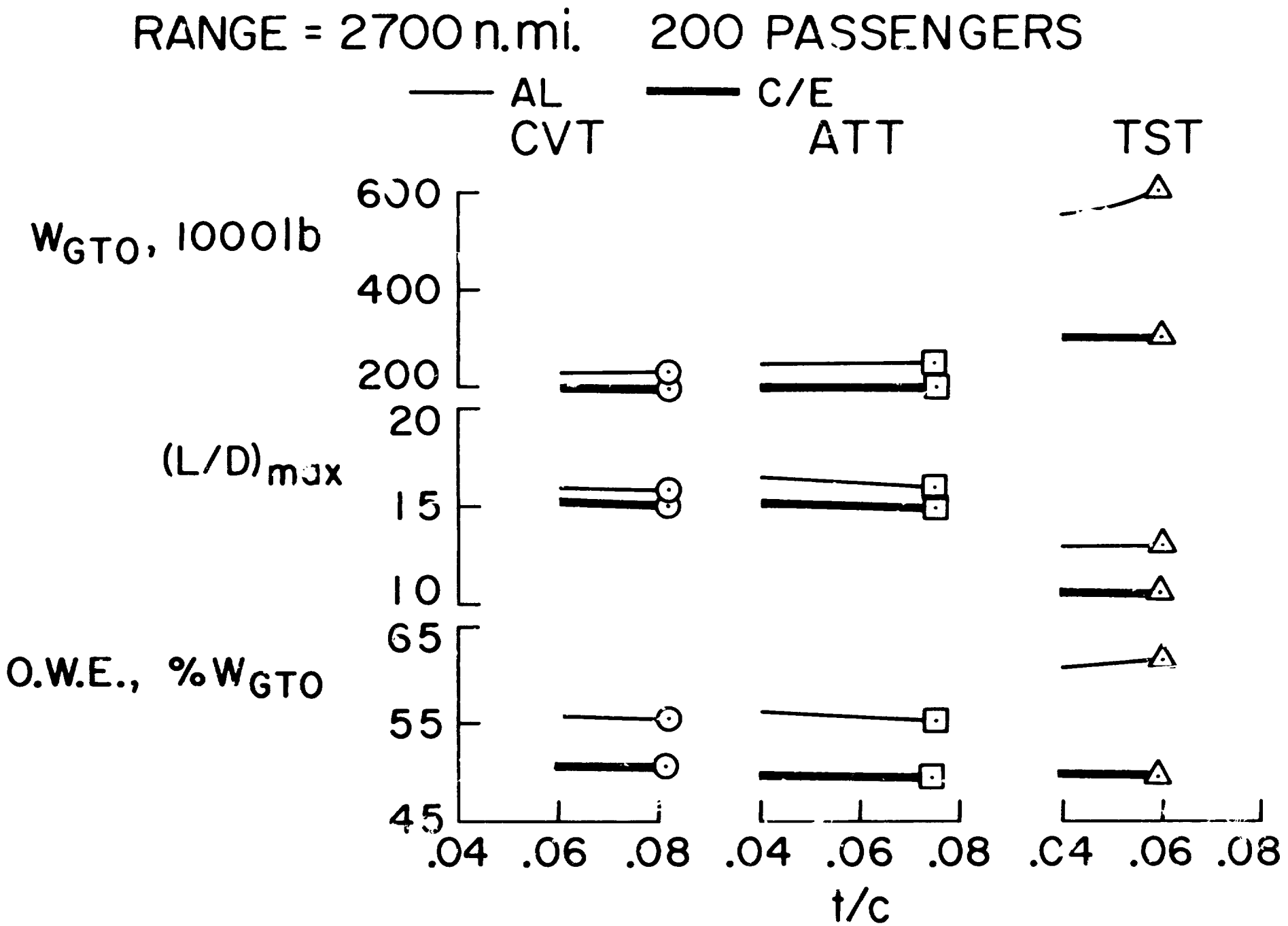

Figure 15. Effect of Thickness-to-Chord on O.W.E., L/D_{max} and Gross Weight

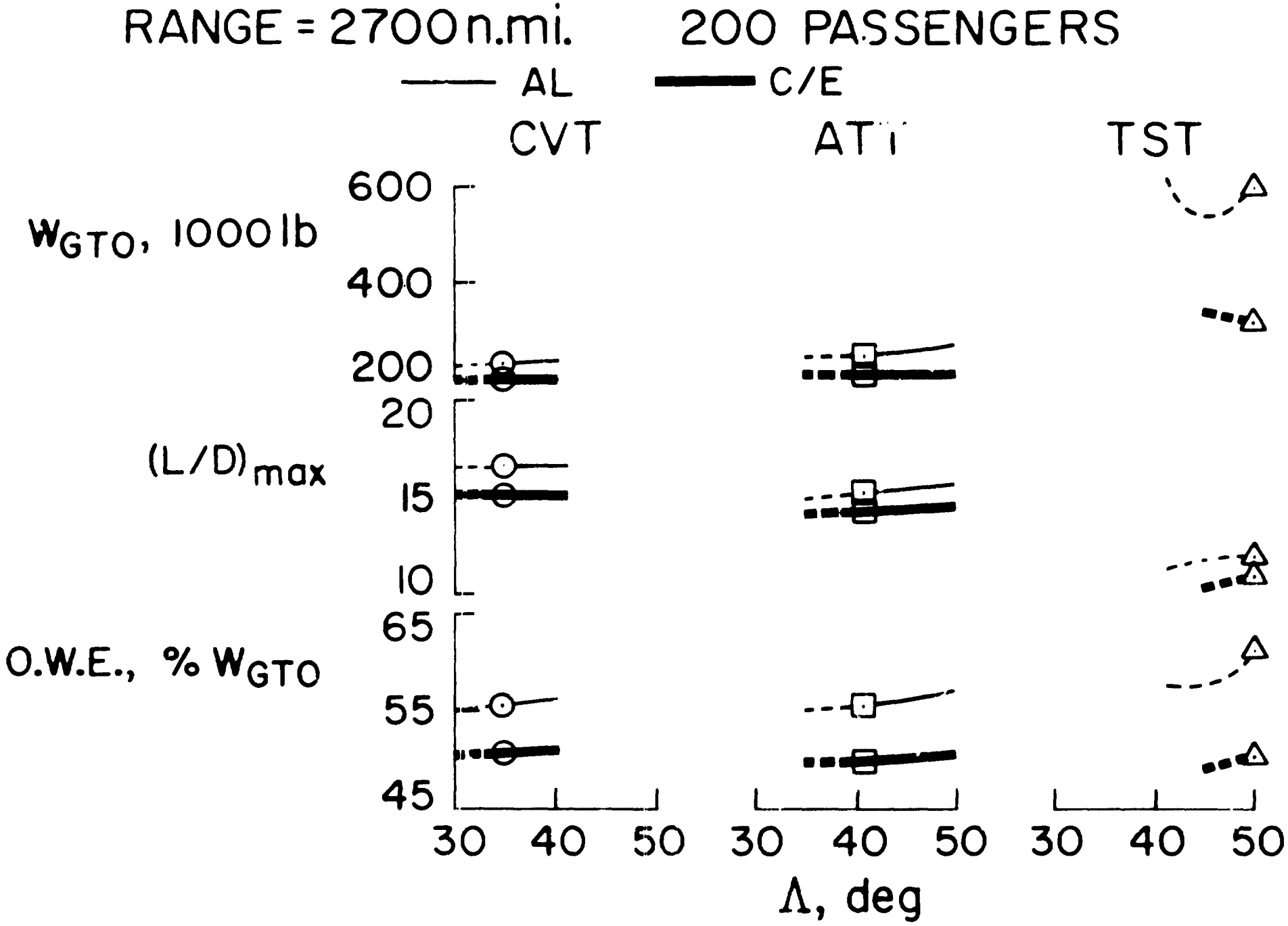

Figure 16. Effect of Sweep on O.W.E., L/D_{max} and Gross Weight

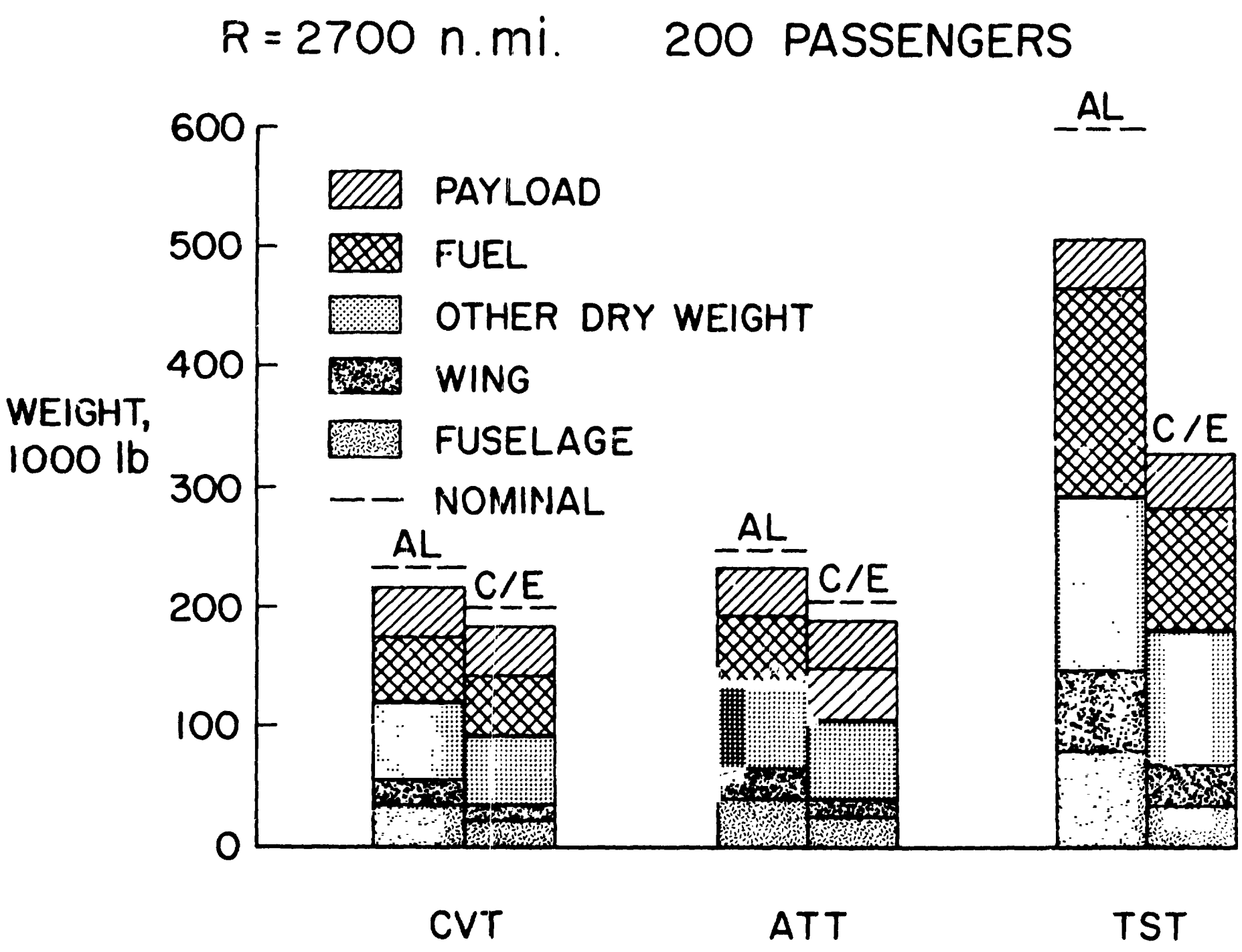

Figure 17. Weights of Optimized Configurations

RANGE = 2700 n.mi. 200 PASSENGERS

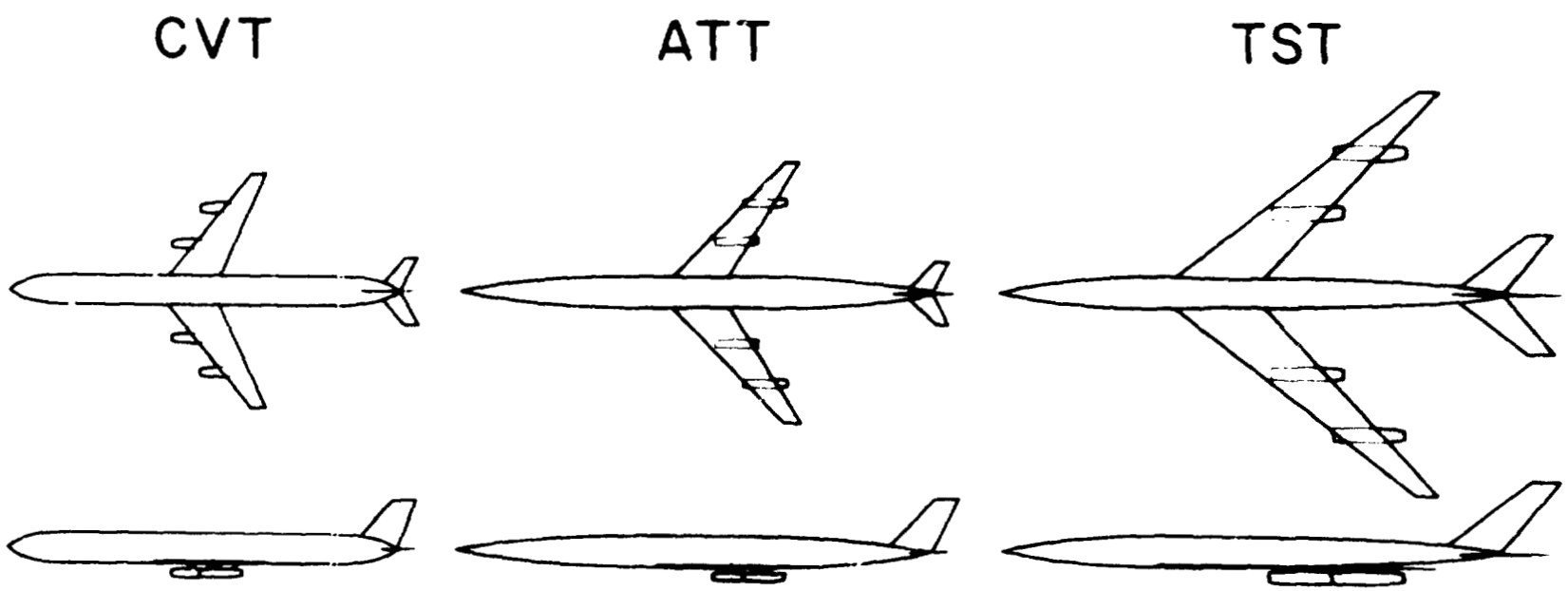

	CVT	ATT	TST
M_{CRUISE}	0.90	0.98	1.15
GROSS WEIGHT	214,500 lb	232,500 lb	504,000 lb
O.W.E. (% W_{GTO})	54.8	57.8	58.2
$(L/D)_{CRUISE}$	15.1	16.3	11.8
$V_{APPROACH}$	160 knots	170 knots	198 knots

Figure 18. Optimum Aluminum Configurations

RANGE = 2700 n.mi. 200 PASSENGERS

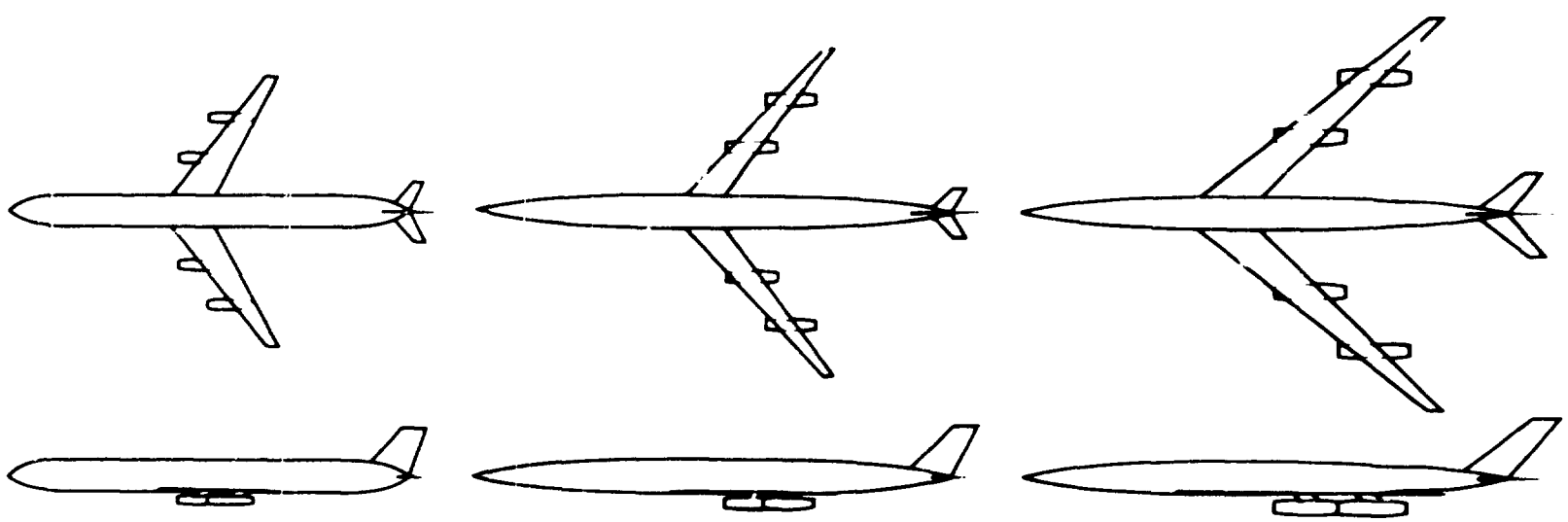

	CVT	ATT	TST
M_{CRUISE}	0.90	0.98	1.15
GROSS WEIGHT	182,500 lb	189,000 lb	323,000 lb
O.W.E. (% W_{GTO})	52.5	55.9	56.0
$(L/D)_{CRUISE}$	16.3	18.6	12.8
$V_{APPROACH}$	148 knots	152 knots	168 knots

Figure 19. Optimum Carbon/Epoxy Configuration

RANGE = 2700 n.mi. 200 PASSENGERS

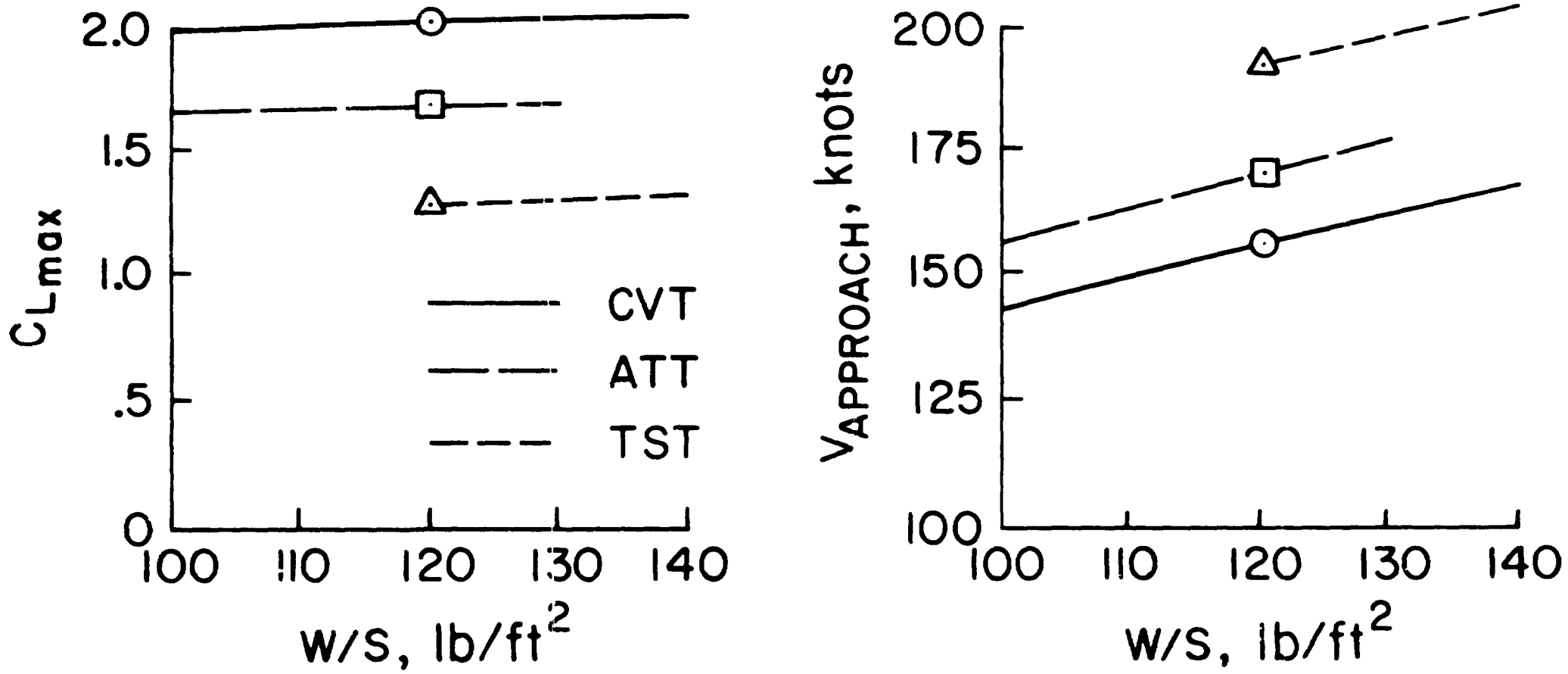

Figure 20. Effect of Wing Loading on $C_{L_{max}}$ and Landing Speed

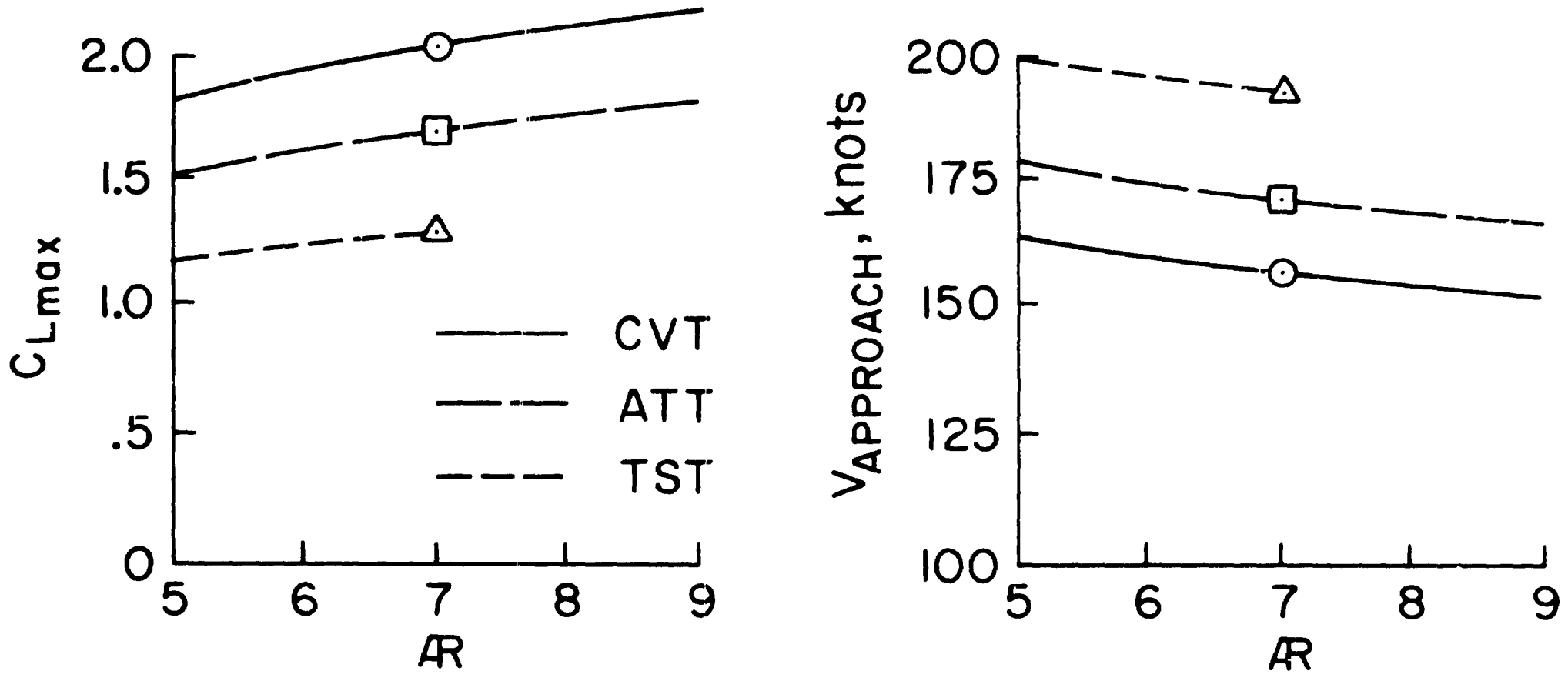

Figure 21. Effect of Aspect Ratio on $C_{L_{max}}$ and Landing Speed

RANGE = 2700 n.mi. 200 PASSENGERS

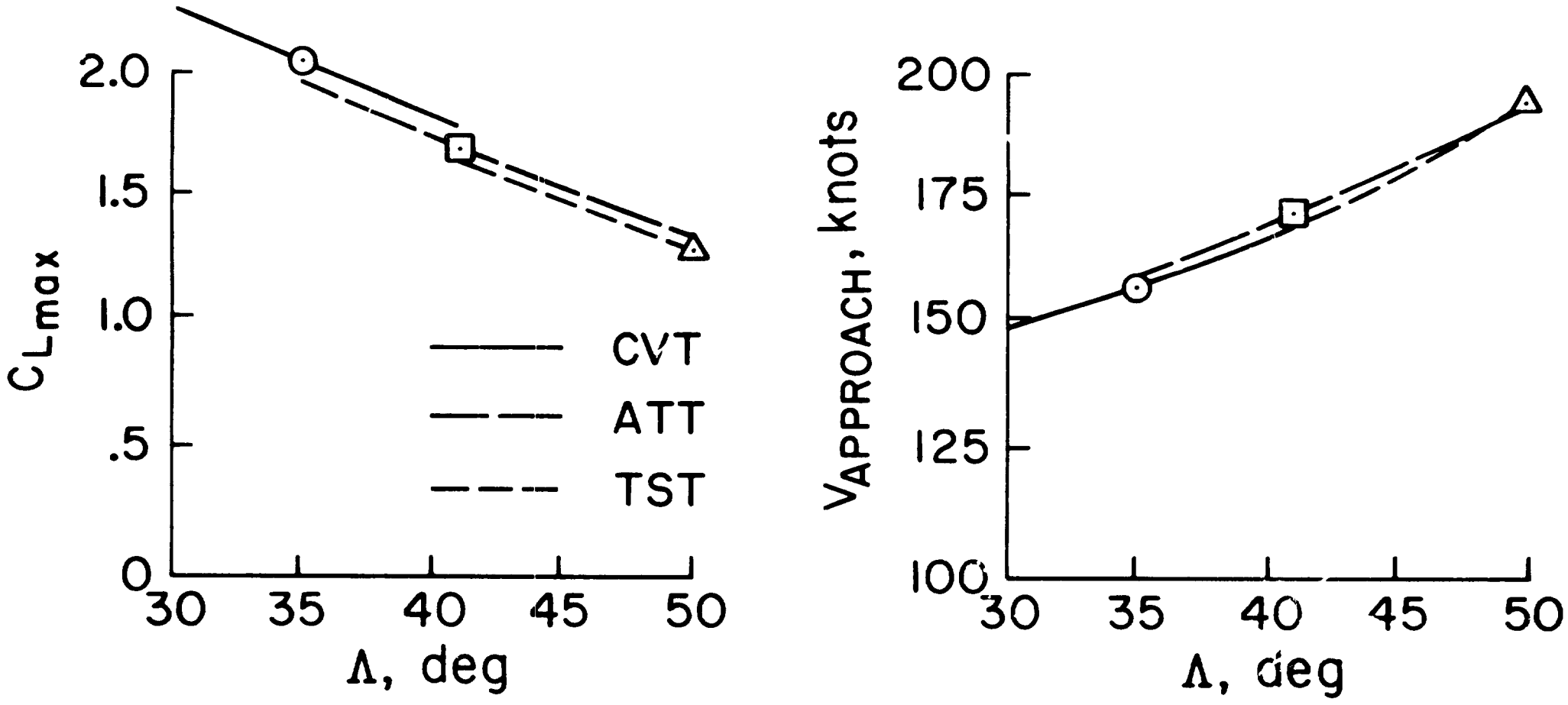

Figure 22. Effect of Sweep on $C_{L_{max}}$ and Landing Speed

RANGE = 2700 n.mi. 200 PASSENGERS

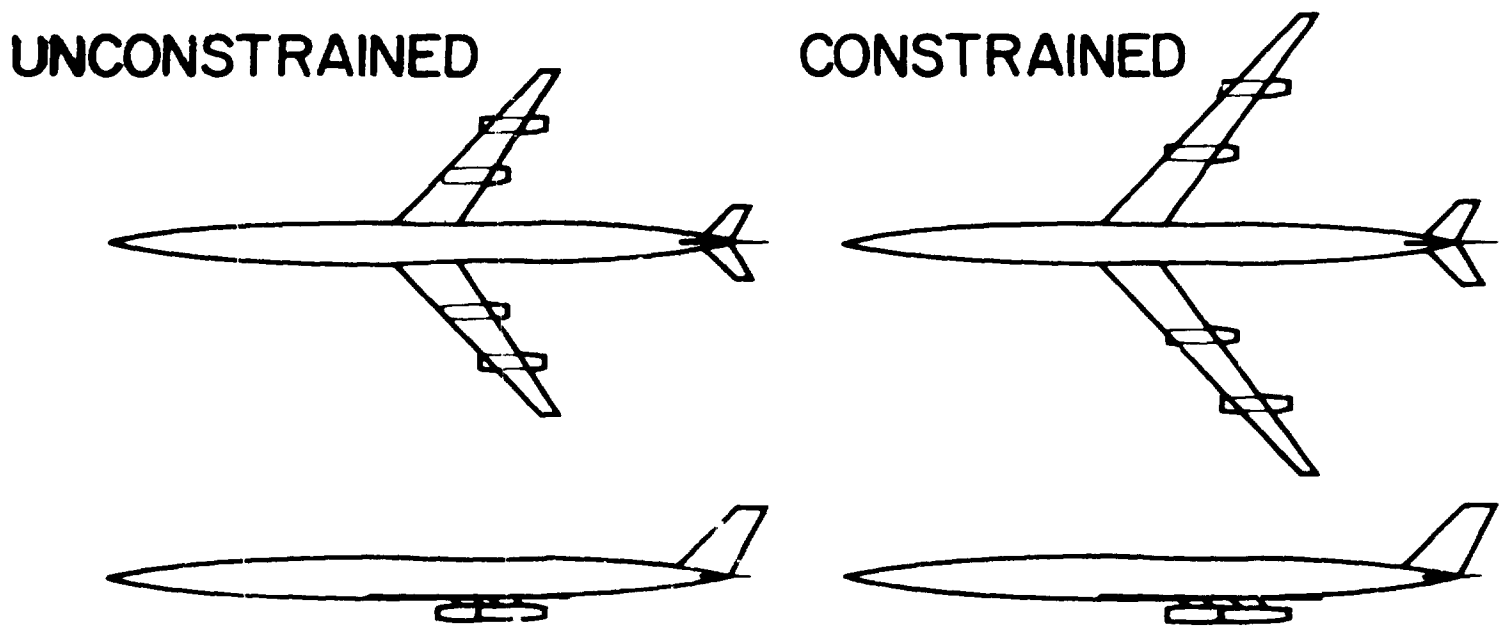

ASPECT RATIO	8.1	11.8
WING LOADING	123 lb/ft^2	101 lb/ft^2
GROSS WEIGHT	232,500 lb	250,000 lb
O.W.E. (%W_{GTO})	57.8	62.2
$(L/D)_{CRUISE}$	16.3	19.7
$V_{APPROACH}$	170 knots	151 knots

Figure 23. Effect of Landing Speed Constraint on Optimum Aluminum ATT Configuration

RANGE = 2700 n.mi. 200 PASSENGERS

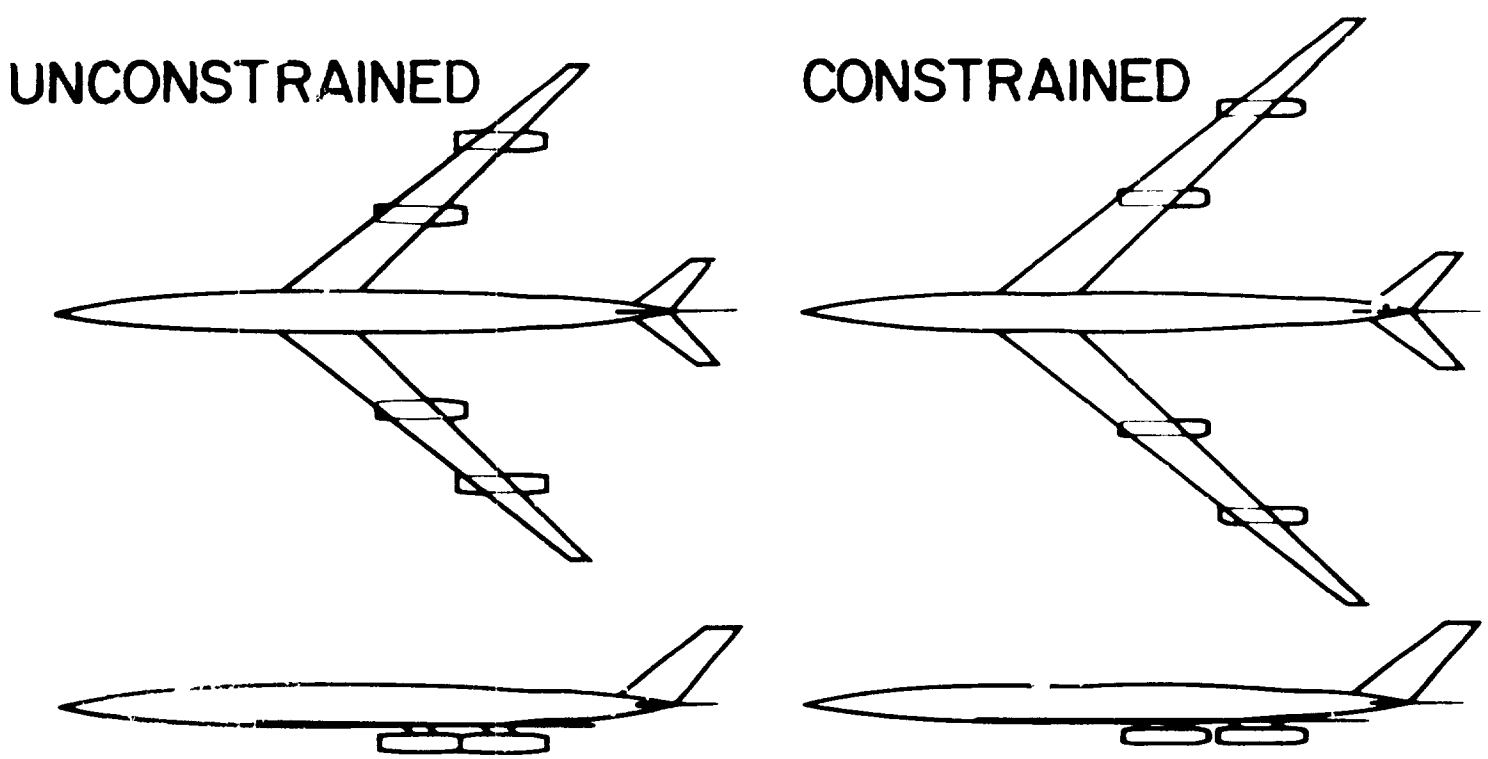

	UNCONSTRAINED	CONSTRAINED
ASPECT RATIO	9.8	11.4
WING LOADING	100 lb/ft^2	89 lb/ft^2
GROSS WEIGHT	323,000 lb	347,000 lb
O.W.E. (%W_{GTO})	56.0	58.3
$(L/D)_{CRUISE}$	12.8	14.3
$V_{APPROACH}$	168 knots	158 knots

Figure 24. Effect of Landing Speed Constraint on Optimum Carbon/Epoxy TST Configuration

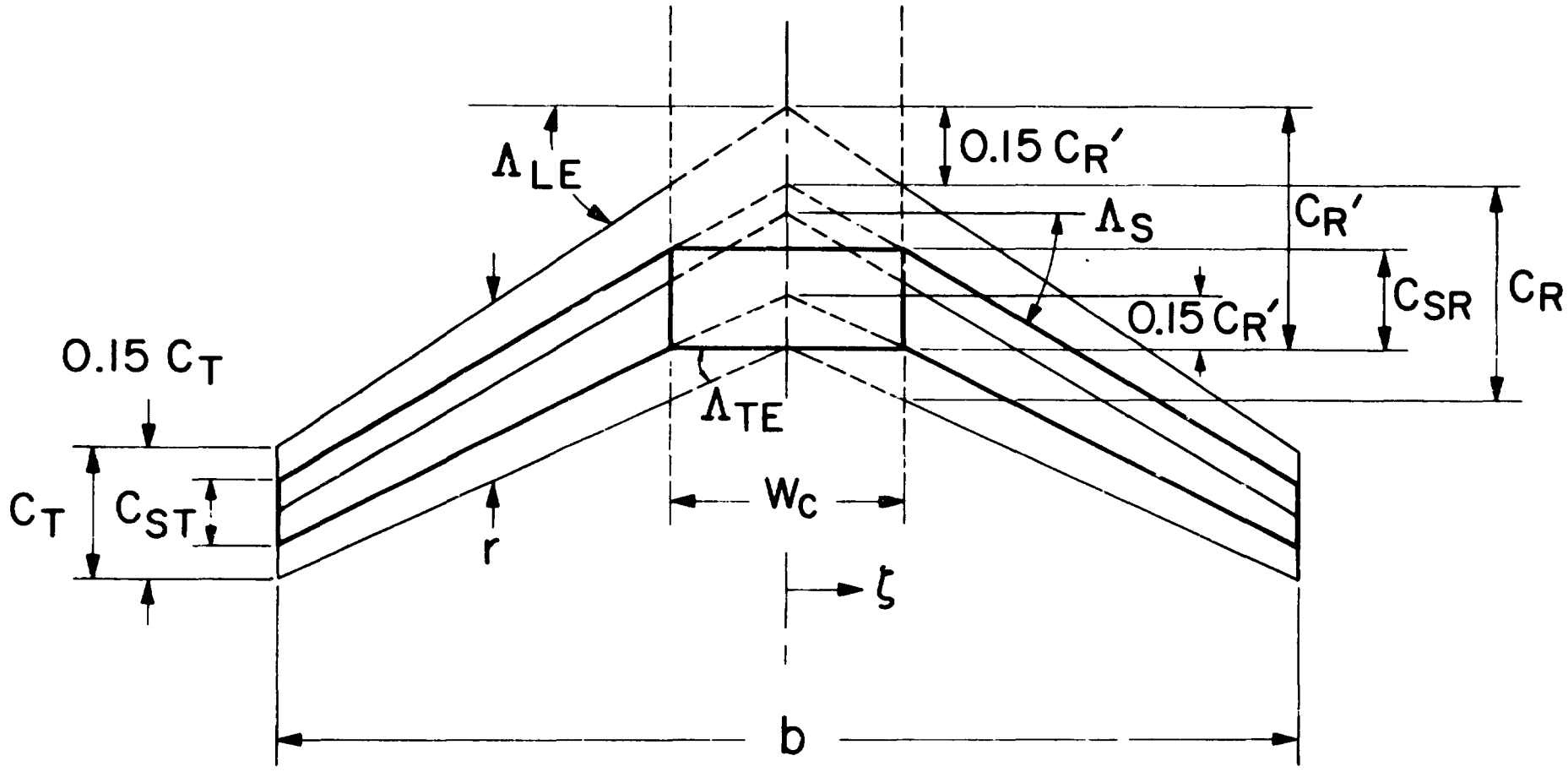

Figure B1. Wing Structural Planform Geometry

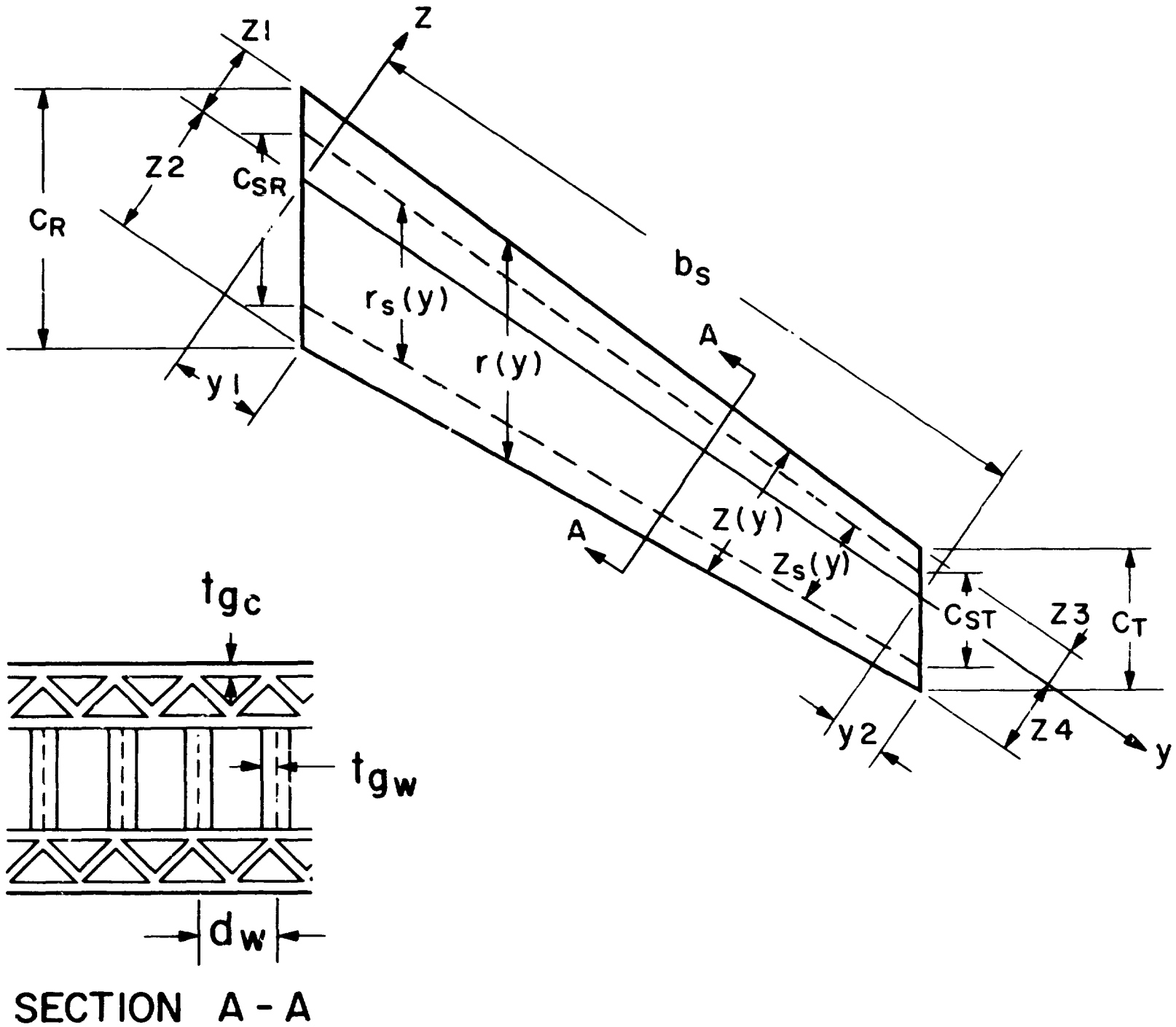

Figure B2. Wing Coordinate System and Structural Concept

"LOCK" WING $\Lambda_{L.E.} = 55°$ $AR = 3.4$ $t/c = 0.06$

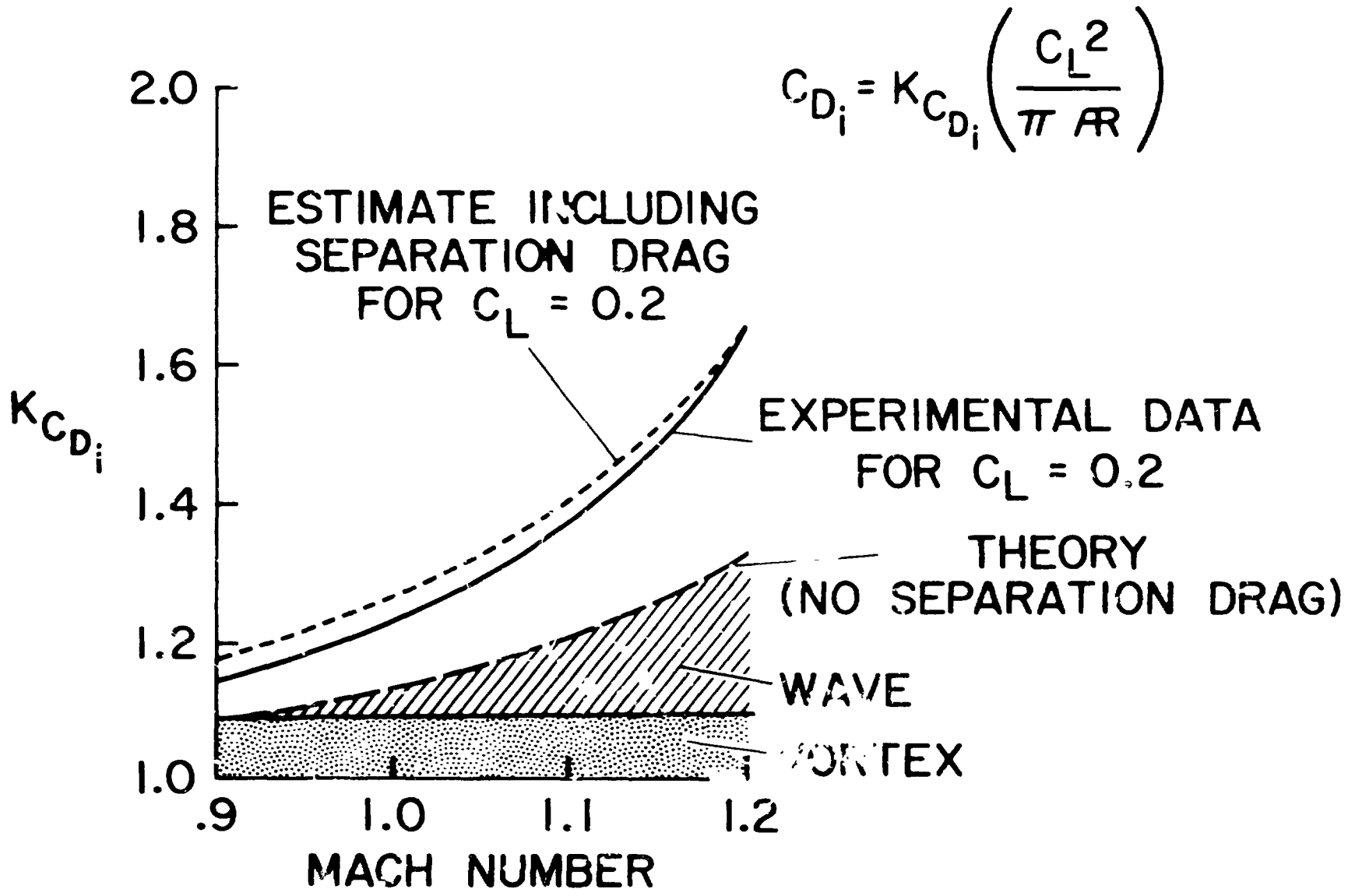

Figure D1. Estimation of Induced Drag

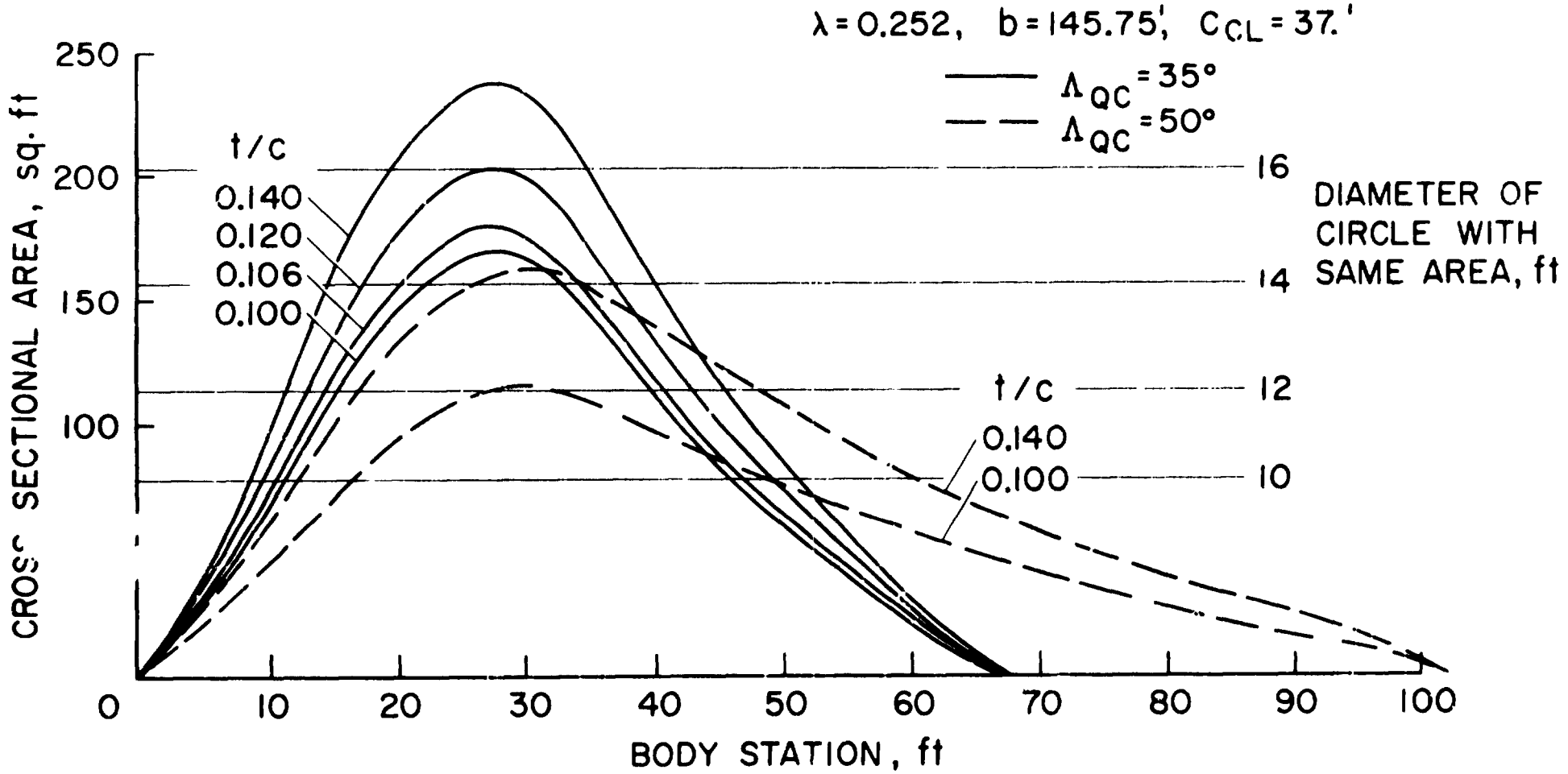

Figure E1. Wing Cross-Sectional Area Distribution

[redacted]

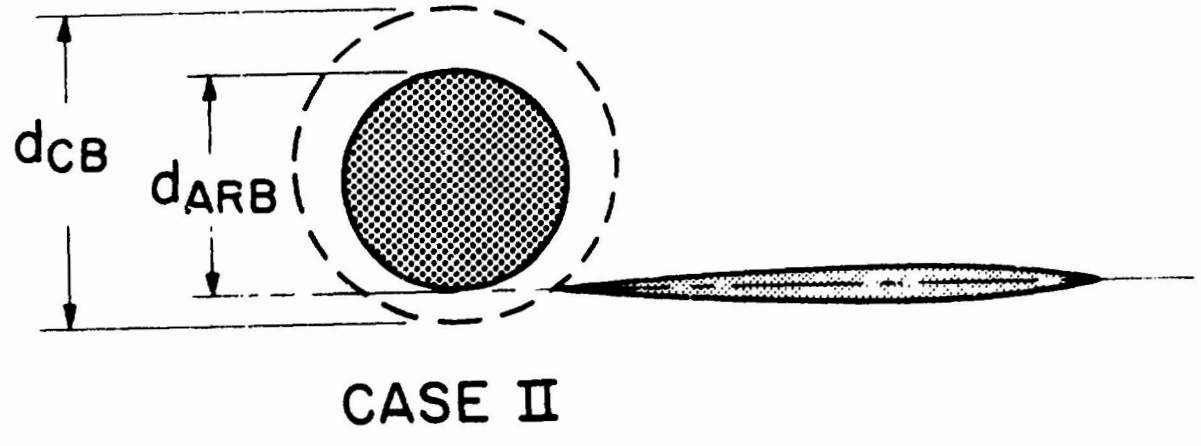

Figure E2. Fuselage/Wing Intersection Geometry Limiting Cases

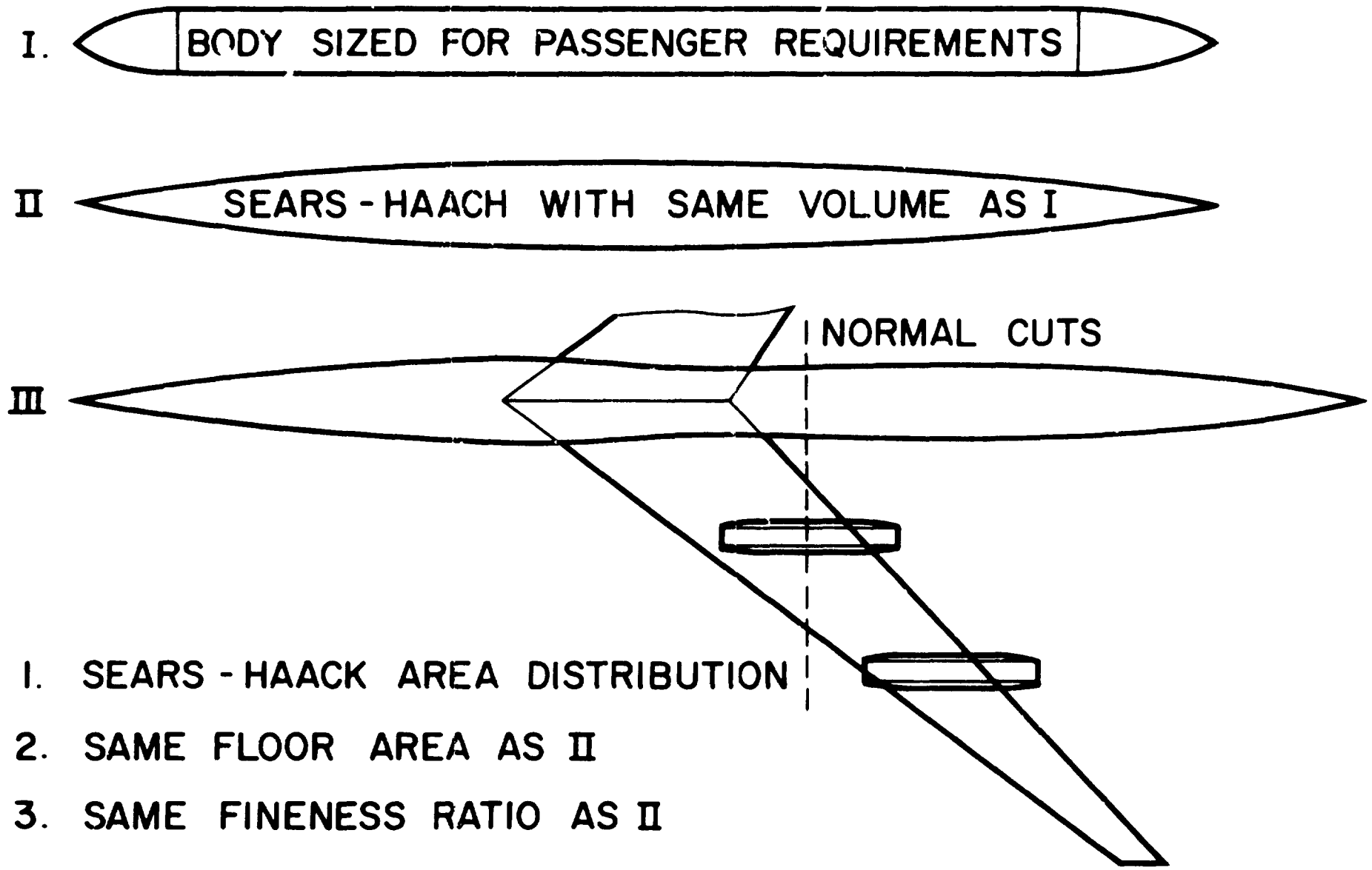

Figure E3. Area Ruling Procedure